DESIGN OF SINGLET FISSION CHROMOPHORES WITH CYCLIC (ALKYL)(AMINO) CARBENE BUILDING BLOCKS

by

Achini Japahuge

A thesis submitted to the Faculty of Graduate and Postdoctoral Affairs in partial fulfilment of the requirements of the degree of

Master of Science

In

Chemistry

Carleton University
Ottawa, Ontario

Abstract

This is a theoretical chemistry study to design singlet fission chromophores. Quantum chemistry methods MRSF-TDDFT and NEVPT2 are used to design chromophores with the building blocks of cyclic (alkyl)(amino)carbenes (CAACs). CAAC dimers with C_2, C_4 and *p*-phenylene spacers are considered. The substitutions with trifluoromethyls and fluorine atoms at the α position are investigated. The electronegative substituents enhance the π accepting capability of the α C, while maintaining it as a quaternary C atom. The phenylene-connected dimers with the two substitutions are identified as promising candidates for the singlet fission chromophores. The cylindrically symmetric C_2 and C_4 spacers allow for substantial structural reorganizations in the S_0-to-S_1 and S_0-to-T_1 excitations. Although the two substituted dimers with the C_4 spacer satisfy (or very close to satisfy) the primary thermodynamics criterion for the singlet fission, the significant structural reorganizations result in high barriers so that the fission is kinetically unfavorable.

Acknowledgement

First of all, I would like to express my sincere gratitude to my supervisor Dr. Tao Zeng for his patient and immense support during my research. I consider myself lucky to work with him and share his knowledge in academic and professional life. My project couldn't have a successful one without him.

I am also grateful to Dr. Seunghoon Lee at Seoul National University and Professor Cheol Ho Choi at Kyungpook National University. They developed the MRSF-TDDFT method that is used to optimize the structures of the designed molecules and calculate their vibrational frequencies.

I would like to thank you all the members who were working with me in the lab, for their support during this time. I would also like to thank you Prof. Robert Crutchley head of the department, who guided us during the seminar sessions that helped me to improve my presentation skills. Also, my heartfelt gratitude goes to Chantelle Gravelle for her immense support on behalf of the administration of the Department of Chemistry.

Further, A very special gratitude goes to the team of Calcul Québec and Compute Canada who provided technical support in terms of calculations and data collecting.

Finally, I am grateful for my family members in Sri Lanka, who have always been supporting me during this time. Thank you all for your encouragement!

Table of Contents

Abstract ii

Acknowledgement iii

List of Abbreviations x

CHAPTER 1 INTRODUCTION 11

Section 1.1 Singlet Fission, an Optoelectronics Phenomenon 11

Section 1.2 Electronic Structure Description of Singlet Fission 13

Section 1.3 The Role of Vibronic Interactions 16

Section 1.4 Searching for Singlet Fission Chromophores 18

Section 1.5 Alternant Hydrocarbons and Diradicals; The Two Limits 20

Section 1.6 A Unified Diradical Character View of the SF Chromophores 22

Section 1.7 Small SF Chromophores 24

Section 1.8 Summary of Promising Theoretical Design 28

Section 1.9 Design of SF Chromophores with Cyclic (Alkyl)(Amino) Carbene Building Blocks, the Motivation and Objective of This Work 29

Section 1.10 Organization of the Rest of the Thesis 31

CHAPTER 2 METHODOLOGY 32

Section 2.1 MRSF-TDDFT Method for Electronic Structure Correlation 32

Section 2.2 Geometry Optimization 33

Section 2.3 Excitation Energy Calculations 34

CHAPTER 3 CALCULATION AND DISCUSSION 36

Section 3.1 The Fluorination and Trifluoromethylation.....36

Section 3.2 CAAC Dimers with a C_2 Spacer 38

Section 3.3 CAAC Dimers with a C_4 Spacer 46

Section 3.4 CAAC Dimers with a *Para*-Phenylene Spacer 54

CHAPTER 4 CONCLUSION 63

Reference.....65

List of Figures

Figure 1. A comparison of photoelectric conversions without (upper panel) and with (lower panel) singlet fission. There are common steps in both panels : (a) photoexcitation, (b) exciton migration, and (c) charge separation between chromophore and acceptor. Steps (d) and (e) are radiationless and radiative decays of singlet exciton. 11

Figure 2. A schematic description of SF. The vertical arrows represent electronic spin. In the state labels, *e* stands for the HOMO-to-LUMO singlet exciton, *t* is the triplet exciton, *g* is the ground state, *c* is the cationic state, and *a* is the anionic state. A vertical dashed line is added to the $t + t$ state to emphasize that the two triplets are independent of each other.....15

Figure 3. (a) Vibrational wave packets on different potential energy surfaces and their transitions to different states in SF; evolutions of diabatic populations in a SF process from dynamics simulations that consider (b) vibronic interaction and (c) only the electronic Hamiltonian. In panel (c), only the ME state population is plotted to show the Rabi oscillation. Panels (b) and (c) are adapted from Ref. 24. 17

Figure 4. Characteristic energy levels of the closed- and open-shell parental structures (at the left and the right end), and their changes when the structures are perturbed towards singlet fission chromophores (in the middle). 21

Figure 5. Weakening of the covalent interaction between two methylene radicals in forming the π bond of ethylene when they contain acceptor (A) and donor (D) substituents. 26

Figure 6. (a) and (b) the σ HOMO and π LUMO of CAAC in its singlet ground state; (c) the π LUMO of CAAC (F). 36

Figure 7. The optimized structures of the (a) S_0, (b) T_1, and (c) S_1 states of $(CAAC)_2$-C_2; (d)-(g) frontier orbitals of the structures of the denoted states; (h)-(i) typical resonance structures of the three states. Some important structural parameters are shown in panels (a)-(c), where the bond lengths are given in Å and the four atoms that define the dihedral angles are highlighted by red circles. In panel (i), only one set of resonance structures are shown for the S_1 state. There is another set which includes the symmetry images of the shown structures. 41

Figure 8. The optimized structures of the (a) S_0, (b) T_1, and (c) S_1 states of $(CAAC)_2$-C_4; (d)-(g) frontier orbitals of the structures of the denoted states; (h)-(j) typical resonance structures of the three states. Some important structural parameters are shown in panels (a)-(c), where the bond lengths are given in Å and the four atoms that define the dihedral angles are highlighted by red circles. In panel (j), only one set of resonance structures are shown for the S_1 state. There is another set which includes the symmetry images of the shown structures. 47

Figure 9. (a) The two singly occupied molecular orbitals $SOMO_1$ and $SOMO_2$ in the T_1 state of $(CAAC)_2$-C_4 and (b) the corresponding localized orbitals obtained from $1/\sqrt{2}(SOMO_1 \pm SOMO_2)$, which are perpendicular π orbitals.....52

Figure 10. HOMO-1 of $(CAAC)_2$-C_4. 53

Figure 11. The optimized structures of the (a) S_0, (b) T_1, and (c) S_1 states of $(CAAC(F))_2$-Ph; (d)-(f) frontier orbitals of the structures of the S_0 state; (g)-(i) typical resonance structures of the three states. Some important structural parameters are shown in

panels (a)-(c), where the bond lengths are given in Å and the four atoms that define the dihedral angles are highlighted by red circles. In panel (i), only some resonance structures are shown for the S_1 state. The others include those with the + and - charges being swapped and those with the symmetry images. 55

Figure 12. Localized orbitals $(CAAC(F))_2$-Ph obtained from $1/\sqrt{2}$(HOMO ± LUMO)....58

Figure 13. Hydrogen bonds of F atoms in (a) $(CAAC(F))_2$-Ph and (b) $(CAAC(TFM))_2$-Ph. The highlighted internuclear distances are given in Å. The red dashed lines indicate F···H hydrogen bonds. 58

Figure 14. A representative structure (a) obtained during the optimization of the S_1 structure of $(CAAC)_2$-Ph and its (b) HOMO and (c) LUMO.....60

List of Tables

Table 1. Excitation energies (in eV) of theoretica\lly designed promising SF chromophores. 28

Table 2. Calculated results for the three C2-connected dimers. All energies are given in eV. 40

Table 3. Calculated results for the three C4-connected dimers. All energies are given in eV. 49

Table 4. Calculated results for the two substituted Ph-connected dimers. All energies are given in eV 56

List of Abbreviations

CAAC Cyclic (alkyl)(amino) Carbene

OPV Organic photovoltaic

SF Singlet Fission

MRSF-TDDFT Mixed Referance Spin-Flip Time-Dependent Density Functional Theory

SF-TDDFT Self Consistence Time Dependent Density Functional Theory

DFT Density Functional Theory

BHHLYP Becke's half-and-half +Lee-Yang-Paar functional

ZPE Zero point Energy

NEVPT2 n-electron valence state perturbation theory 2

CAAC(F) Fluorinated Cyclic (alkyl)(amino) Carbene

CAAC(TFM) Trifluoromethylated Cyclic (alkyl)(amino) Carbene

NHC N-heterocyclic Carbene

HOMO Highest Occupied Molecular Orbital

LUMO Lowest Unoccupied Molecular Orbital

XRD X-Ray Diffraction

Dipp Diisopropylphenyls

LUNO Lowest Unoccupied Natural Orbital

SOMO Singly Occupied Molecular Orbital

Ph *para*-phenylene

CHAPTER 1 INTRODUCTION

Section 1.1 Singlet Fission, an Optoelectronics Phenomenon

Singlet fission is an interesting optoelectronics phenomenon that can enhance photoelectric conversion efficiency in organic photovoltaic devices. In a conventional organic photovoltaic device, the absorption of a solar photon in the chromophore layer generates a singlet exciton. We label this excitonic state as S_1 for its character of the lowest (1) singlet (S) excited state of the chromophore molecule. Such an exciton can hop to the chromophore–acceptor interface, where the exciton undergoes charge separation to a hole and an electron. The holes and electrons are accumulated in electrodes and become free charge carriers.

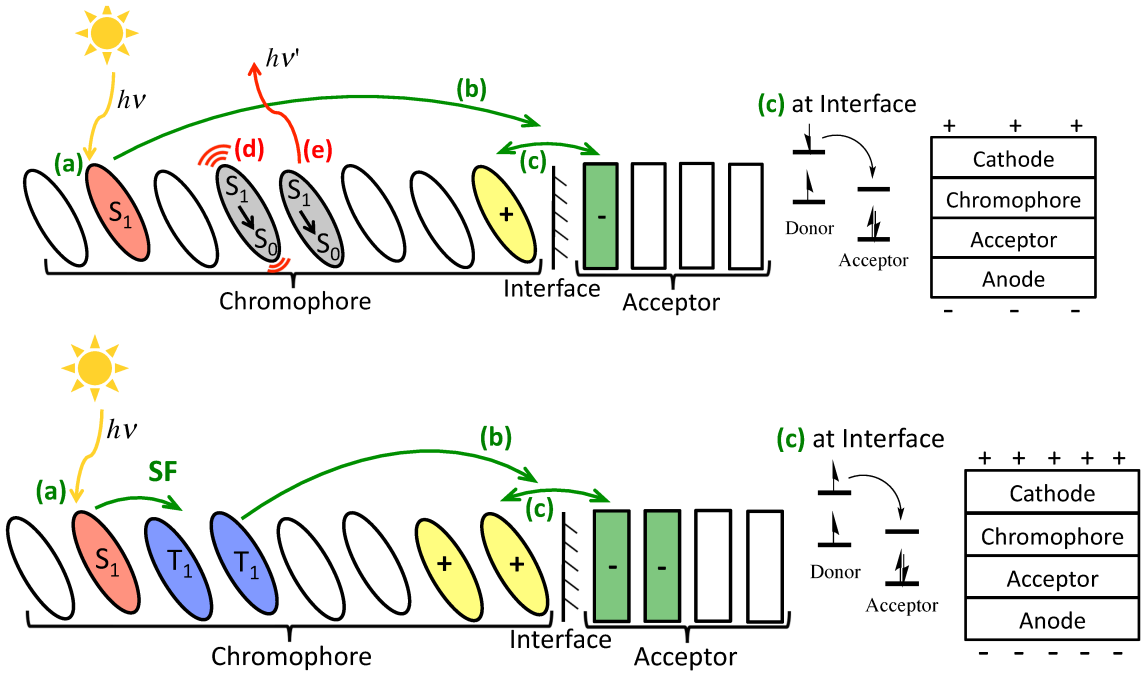

Figure 1. A comparison of photoelectric conversions without (upper panel) and with (lower panel) singlet fission. There are common steps in both panels : (a) photoexcitation, (b) exciton migration, and (c) charge separation between chromophore and acceptor. Steps (d) and (e) are radiationless and radiative decays of singlet exciton.

However, the S_1 exciton can undergo radiative and radiationless decays to the ground state (labeled as S_0), lowering the photoelectric conversion efficiency. All these steps are demonstrated in the upper panel, where the S_1 exciton is simplified to be localized in one chromophore molecule. In reality, the singlet exciton is delocalized and the range of delocalization is correlated with the bandwidth of the excitonic states, that is, singlet exciton transfer integrals.

Singlet fission (SF) is the process in which one S_1 exciton shares its energy with an adjacent chromophore that is in the ground state and converts to two triplet excitons on the two chromophores.[1,2] The triplet excitons are labeled as T_1. SF starts with an internal conversion process, which typically occurs on a sub-ps to ps timescale[3-7] and outcompetes the S_1 radiative and radiationless decays, which usually occur on ns timescales or longer. Molecules with ultrafast S_1- to-S_0 radiationless decay, for example, azulene,[8] are not appropriate SF chromophores. The number of excitons is doubled in SF. Furthermore, owing to the spin selection rule, the T_1 excitons have a longer lifetime than S_1. The doubled number and longer lifetime enable more excitons to reach the interface and undergo charge separation, giving more electrons and holes at the electrodes. Therefore, SF provides an avenue to enhance photoelectric conversion efficiency. In their qualitative analysis, Hanna and Nozik showed that with SF, the conversion efficiency can surpass the approximately 1/3 Schockley–Queisser limit[9] of a single junction solar cell and reach approximately 1/2.[10] Indeed, organic photovoltaic (OPV) devices that exhibit > 100 % quantum efficiency (electrons/photons ratio) have been fabricated,[11-14] and the generation of more than one electron–hole pair by absorbing one photon is enabled by

SF. A tandem architecture with a blue-absorbing SF donor and a red-absorbing acceptor is ideal for third generation solar cells.[1,10,15,16]

Section 1.2 Electronic Structure Description of Singlet Fission

A SF process is schematically depicted in Figure 2, in which a dimer model of chromophores A and B is used. As the triplet pair resides on two chromophores, dimers are the smallest systems that can have SF. They can be covalently connected dimers or two adjacent molecules in a van der Waals solid. In each chromophore, only the highest occupied and the lowest unoccupied molecular orbitals (HOMO and LUMO) are considered. A SF process consists of two steps, the spin-conserved step and the spin-disentangled step. The spin-conserved step occurs within the singlet spin manifold and involves five electronic states:[1,2] the single-excitonic states *eg* and *ge*, which are generated by photoexcitation; *tt*, a singlet-coupled triplet pair state; and the charge-transfer (CT) states *ca* and *ac*. The vertical arrows (electronic spins) and horizontal bars (orbital levels) in Figure 2 indicate occupation schemes and characteristic spin alignments of the states.

The second step shown in Figure 2 is the spin-disentangled step, in which the triplet pair loses its spin-coupling as an overall singlet and becomes two independent triplet states with random orientations. This step is induced by spin-dependent Hamiltonians, for example, the dipole–dipole interaction between electronic spins and the electron–nuclear spin interaction.[1,17,18] These Hamiltonians do not commute with the total electronic spin operator. They mix the singlet-coupled triplet-pair state with the triplet- (if allowed by symmetry[1]) and quintet-coupled analogs. Along with thermalization, they

randomize the orientations of the two triplets. These interactions are very weak, typically < 1 cm^{-1} in magnitude. This makes the disentanglement a slow process. A recent study that employed both transient absorption and time-resolved electron spin resonance spectroscopic techniques on 6,13-bis(triisopropylsilylethynyl)-pentacene (TIPS-pentacene) covalent dimers showed that it took hundreds of nanoseconds to lose the spin correlation of the triplet pair.[19] Similar experimental techniques were employed to study the 6,13-bis(triisobutylsilylethynyl)-pentacene dimer with a nonconjugated linker.[20] It took hundreds of nanoseconds for the singlet-coupled triplet pair to convert to the quintet-coupled triplet pair, which is consistent with the findings in Reference 19. Furthermore, it took several microseconds to generate independent triplet excitons. The spin-disentanglement is so slow that the triplet states may have migrated apart, yet their spins are still correlated. Because of the small magnitude of the spin-dependent interactions, (pseudo)degeneracy of the singlet-, triplet-, and quintet-coupled triplet-pair states is necessary for the spin-disentanglement. When the two triplets reside on adjacent molecules, they may be ferromagnetically or antiferromagnetically coupled and the three spin manifolds are of different energies, hindering the disentanglement. When they dissociate to be nonadjacent, the (anti)ferromagnetic coupling is ineffective and the degeneracy is achieved. Therefore, dissociation facilitates the spin-disentanglement.

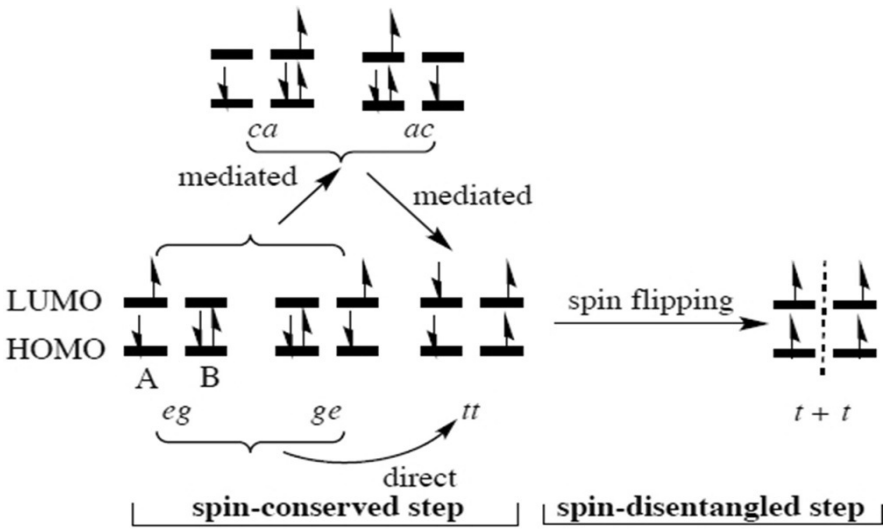

Figure 2. A schematic description of SF. The vertical arrows represent electronic spin. In the state labels, *e* stands for the HOMO-to-LUMO singlet exciton, *t* is the triplet exciton, *g* is the ground state, *c* is the cationic state, and *a* is the anionic state. A vertical dashed line is added to the *t* + *t* state to emphasize that the two triplets are independent of each other. This figure is taken from Ref. 80.

We need to emphasize that Figure 2 gives a simplified description of SF. It is most relevant for SF across a dimer. It cannot describe the delocalization of the single-excitonic state beyond two monomers, neither the migration of the triplets. Also, the CT states may have different energies when the two chromophores are immersed in a solid environment. Another important difference is in the number of states (or density of states). In a dimer, there are two single-excitonic states and one multi-excitonic state. As the size of the oligomer grows, the number of single-excitonic states grows linearly, whereas that of multi-excitonic states grows quadratically. In combination with triplet migration, this faster growth of multi-excitonic states provides an entropy driving force for SF.

Section 1.3 The Role of Vibronic Interactions

SF is an energy transfer process. Like in other energy transfer processes, vibronic coupling plays a significant role in SF. The five diabats and their analogs in more extended systems can be viewed as forming the electronic system, which is coupled to a bath of vibrational degrees of freedom (phonons in solids).[21] Thermodynamically speaking, the bath dissipates the energy released in the SE-to-ME conversion if it is an exoergic process. For an endoergic SF process, which can still be driven by entropy,[7,22] the bath provides the needed energy.

The couplings of the diagonal matrix elements are called the Holstein couplings, and those of the off-diagonal elements are called the Peierls couplings.[23] The Holstein couplings bring about different potential energy surfaces (PESs) for different diabats. Figure 3 (a) demonstrates the effects of Holstein couplings in an ideal SF process. The Franck–Condon excitation (*hv*) vertically shifts the ground-state (GS) vibrational wave function to the SE potential energy surface (simplified as a curve in the figure, with an abstract vibrational coordinate q). The ground-state structure corresponds to an interaction region where the SE and ME energies are close and the SE-to-ME transition induced by the matrix element $H_{SE,ME}$ is efficient, resulting in a vibrational wave packet on the ME PES. $H_{SE,ME}$ is assumed to be fixed in this model. The back-and-forth population conversion between SE and ME, which is the Rabi oscillation, continues. Meanwhile, the wave packets on the different PESs evolve following the respective potentials and migrate away from the vertical interaction region. All wave packets in the figure are simplified as gaussians. Given that the ME PES has a minimum lower than the

SE PES, the ME wave packet explores structures with larger SE–ME energy gaps than the SE wave packet. Consequently, the ME-to-SE conversion is slower than the SE-to-ME conversion. The efficiency of a $H_{SE,ME}$-driven conversion is reflected by the transparency of the relevant arrow in Figure 3 (a): the more transparent, the slower. These unbalanced conversion rates remove the Rabi oscillation and result in an overall unidirectional SE-to-ME conversion. Naturally, as the number of the coupling modes, that is, the dimension of the PESs, increases, the conversion is less reversible. Again, the argument here is based on the dimer model. The entropy effect that favors the formation of the ME state has not been considered yet.

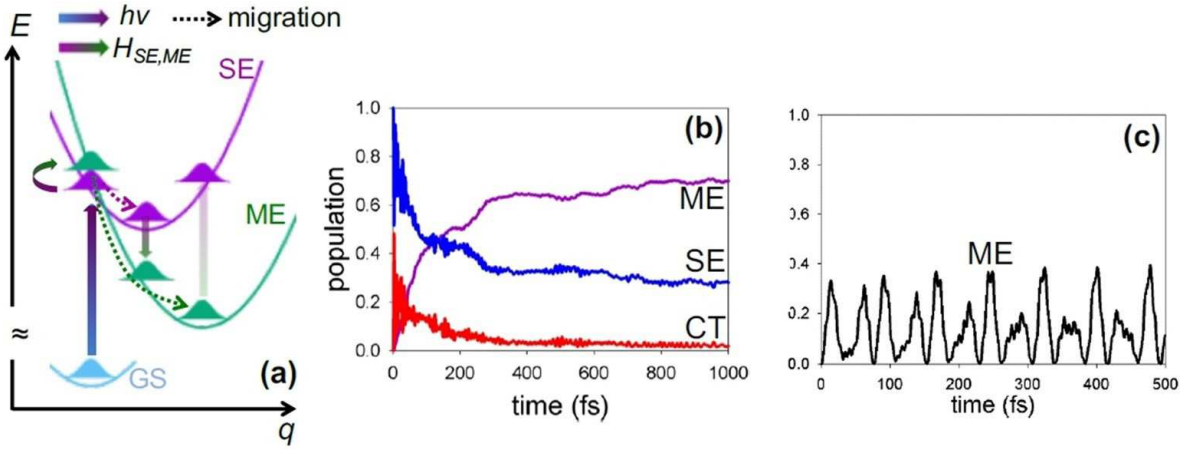

Figure 3. (a) Vibrational wave packets on different potential energy surfaces and their transitions to different states in SF; evolutions of diabatic populations in a SF process from dynamics simulations that consider (b) vibronic interaction and (c) only the electronic Hamiltonian. In panel (c), only the ME state population is plotted to show the Rabi oscillation. Panels (b) and (c) are adapted from Ref. 24.

The significant distance between minima in PESs leads to a small overlap between the SE and ME wave packets, that is, a decoherence between the two states. The decoherence provides another way to understand why vibronic coupling destroys the

Rabi oscillation.[24] If the Franck–Condon region is far from the interaction region, the Holstein coupling may bring the SE wave packet to the interaction region. Typical evolutions of populations in SF from dynamics simulations with and without considering vibronic interactions are compared in Figure 3 (panel (b) vs. panel (c)). As elucidated above, the former exhibits a unidirectional SE-to-ME population conversion whereas the latter shows a Rabi oscillation. Evidently, there is no SF if there are no vibronic couplings.

Section 1.4 Searching for Singlet Fission Chromophores

SF was first observed in crystalline anthracene (**1**) in 1965[25] and its studies were immediately extended to tetracene (**2**) and pentacene (**3**).[26-31] A few materials are known to undergo SF efficiently. They include tetracene, pentacene, some of their derivatives,[4,6,7,11,12,32-43] perylene diimide,[44] as well as several conjugated polymers.[45-50] An emerging class of SF chromophores are non-polycyclic thienoquinoid compounds.[51] This highly limited arsenal of SF chromophores obstructs the application of SF in OPVs. This difficulty motivated a series of studies in understanding the intrinsic characters of the chromophores and searching for new chromophores.

The key energetic requirements for SF chromophores are,

$$E(S_1) \geq 2E(T_1) \quad (1)$$

$$E(T_2) \geq 2E(T_1) \quad (2)$$

$$E(Q_1) \geq 2E(T_1) \quad (3)$$

S, T and Q are used to label states in singlet, triplet and quintet spin manifolds. The subscripts 1 and 2 indicate the first and second excited states in the respective spin manifolds. The first inequality guarantees that the fission of one S_1 exciton to two T_1 excitons is exoergic and thermodynamically favorable. The second

inequality ensures that the fusion of two SF generated T_1 excitons to one T_2 exciton is endoergic and thermodynamically unfavorable. In terms of spin angular momentum addition, two T_1 excitons can also fusion to one Q_1 exciton (the lowest quintet excited state). However, $E(Q_1)$ is usually greater than $2E(T_1)$ and the fusion is hindered as shown in the last inequality.

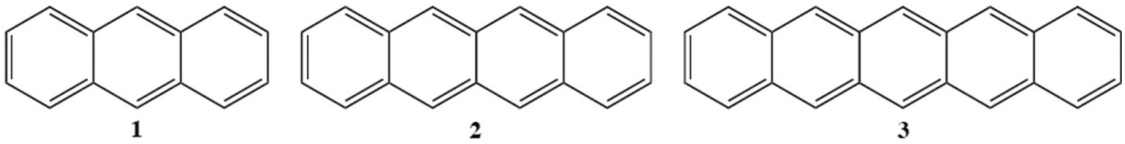

1 2 3

T_1 typically involves exciting an electron from HOMO to LUMO and flipping its spin, whereas Q_1 involves the second excitation and spin-flipping from HOMO-1 to LUMO+1, which costs more energy than the first excitation. Therefore, Equation (3) is usually satisfied and can be ignored. Two T_1 excitons are unlikely to recombine to one molecule in T_1 and one molecule in S_0 owing to the substantial energy release by $E(T_1)$ (i.e., the energy gap law). Instead, they may recombine to form one molecule in T_2 and the other in S_0; $E(T_2)$ might be close to $2E(T_1)$. Equations (1) and (2) guide the search for SF-capable chromophores. As S_1 usually involves HOMO-to-LUMO excitation (Class I chromophores defined in Ref. [1]) whereas T_2 involves excitation with a larger orbital energy gap, for example, HOMO-to-LUMO+1, HOMO-1-to-LUMO, etc., $E(T_2)$ is likely to be larger than $E(S_1)$. Therefore, we can by and large focus on Equation (1). However, $E(T_2)$ should always be examined in designing SF chromophores. In addition to Equation (2), $E(T_2) > E(S_1)$ is desired.[1,2] This inequality ensures a thermodynamically unfavored S_1-to-T_2 intersystem crossing (ISC), which is followed

by the efficient T_2-to-T_1 decay (Kasha's rule[52]); only one T_1 exciton results. Although $E(T_2) > E(S_1)$ is desired, it is not as a strong condition as Equations (1) and (2). The states involve p- to-p excitations. According to El-Sayed's rule,[53,54] ISC between π excited states is usually slow, although it may be thermodynamically favorable. The energies in Equations (1) to (3) should be those of the optimized structures of the respective states, because vibrational relaxation is competitively fast compared with the fission and fusion. Other than the energy relations, $E(T_1)$ close to 1 eV is desired. This gap maximizes the efficiency in energy conversion.[1]

One usually does not need to consider states higher-lying than those in Eqs. 1-3. According to the Kasha's rule, those higher-lying states (S_3, T_3, Q_2, etc.) are usually short-lived. They decay to the lower-lying excited states rapidly through non-adiabatic vibronic interaction.

Section 1.5 Alternant Hydrocarbons and Diradicals; The Two Limits

The structural search has been concentrated on π-conjugated systems because of their good absorption in an extensive range of photon frequencies. The first systematic search for chromophores that satisfy Equation (1) was performed by Paci et al.[55] They proposed two classes of parental structures that can be modified to meet the requirement: the closed-shell alternant hydrocarbons in the left side of Figure 4 and the open-shell diradicals in the right side. When both S_1 and T_1 involve one-electron HOMO-to-LUMO excitation, their energies differ by twice the exchange integral between the two orbitals ($2K_{hl}$). For alternant hydrocarbons, this gap is largely invariant.[1] Therefore, by reducing $E(S_1)$ (or likewise the HOMO–LUMO gap), we will

eventually reach the structures that satisfy $E(S_1) \geq 2E(T_1)$. Indeed, as the length of acene increases and the HOMO–LUMO gap decreases,[56] all acenes longer than and including tetracene satisfy this condition. At the other end, diradicals have triplet ground states, whereas the lowest singlet (S_0) is higher by twice the exchange integral between the two singly occupied orbitals A and B ($2K_{AB}$). $E(S_1) \geq 2E(T_1)$ is automatically satisfied. However, diradicals are in general unstable. By increasing the overlap between orbitals A and B, and hence the HOMO–LUMO gap (HOMO:the bonding orbital between A and B; LUMO : antibonding), the resultant more stable diradicaloid has S_0 as the ground state and $E(T_1)$ increases. When $E(T_1)$ increases to near but still less than $\frac{1}{2}E(S_1)$, a promising SF chromophore is reached. The two classes of structures are not mutually exclusive, as the HOMO–LUMO gap and diradical character are correlated.[56-58]

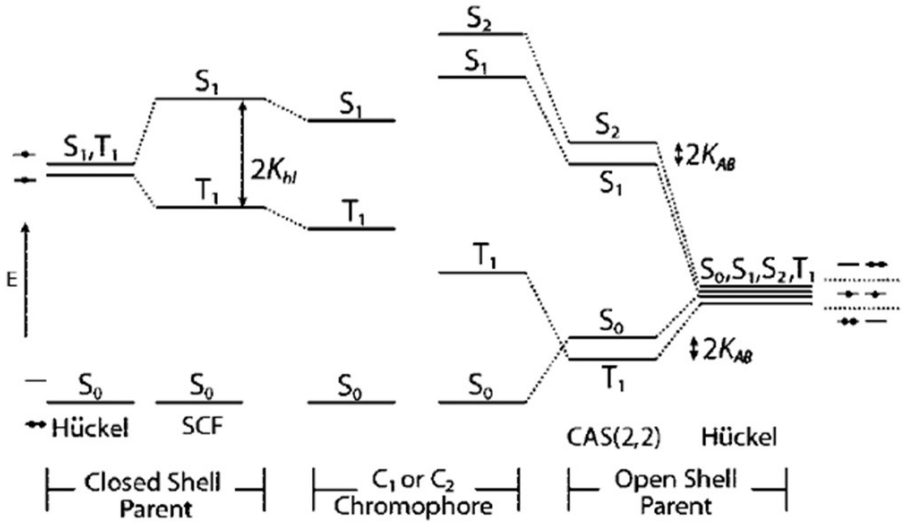

Figure 4. Characteristic energy levels of the closed- and open-shell parental structures (at the left and the right end), and their changes when the structures are perturbed towards singlet fission chromophores (in the middle). This figure is taken from Ref. 1.

Paci et al. used the efficient Pariser–Parr–Pople (PPP) method[59,60] to calculate geometrically relaxed $E(S_1)$, $E(T_1)$, and $E(T_2)$ values for more than 60 structures of the two classes. Several *o*- and *p*-xylylene derivatives were predicted to be promising chromophores. Among them, 1,3-diphenylisobenzofuran (**4**, DPB) has been shown to undergo SF.[61,62,63] DPB is the first theoretically designed chromophore that turned out to undergo SF. It has attracted lots of research interest.[61-65]

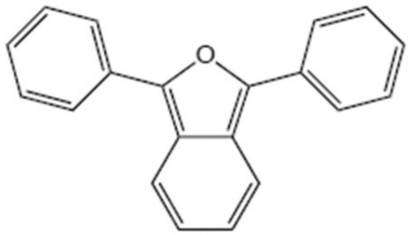

4

Section 1.6 A Unified Diradical Character View of the SF Chromophores

Considering the close connection between the two classes of parental structures for SF chromophores, Minami and Nakano developed a unified view for searching for SF chromophores based on multiradical character.[66] They used a simple linear H_4 model of $D_{\infty h}$ symmetry to investigate the relationship between excitation energies and diradical/tetraradical character. Such a model with four orbitals and four electrons (4o4e) allows to simulate the T_2 state of a chromophore. By varying the three H-H internuclear distances, they freely tuned the ground-state character of the H_4 model from a perfect closed- shell (H-H···H-H), to a diradical (H···H-H···H), and to a tetraradical (H···H···H···H). $E(S_1)$-$2E(T_1)$ and $E(T_2)$-$2E(T_1)$ were calculated for each H_4 conformation and plotted against the occupation numbers (y_0 and y_1) of the lowest unoccupied natural orbital (LUNO) and the second lowest one (LUNO+1), which,

respectively, indicate the diradical and tetraradical characters of a molecule. Through inspecting the variations of the two differential energies with respect to y_0 and y_1, the authors proposed the following guidelines for the chromophore search: 1) the chromophore should have considerable but not too much diradical character in order to satisfy $E(S_1)$-$2E(T_1)$ greater than and close to 0, so that the energy efficiency in SF is high; 2) the tetraradical character of a chromophore should be minute to satisfy $E(T_2)$-$2E(T_1) > 0$.

The diradical character can be enhanced by increasing the aromaticity of a fragment of a molecule. Ito and Nakano investigated a series of heteroacene models based on core structures of *m*-xylylene (N*m*-*i*, **5**).[67] The authors tuned the aromaticity of the central rings by N-substitution (changing the *m* value) and modified the π-conjugation extension (changing the *i* value). The increases of the aromaticity and conjugation length of the central rings strengthen the diradical character with the resonance structure shown in **5**, and the model molecules start to satisfy Equation (1). N2-4 and N0-3 were identified as ideal SF chromophores: they satisfy the energy criteria and have $E(T_1)$ close to 1 eV.

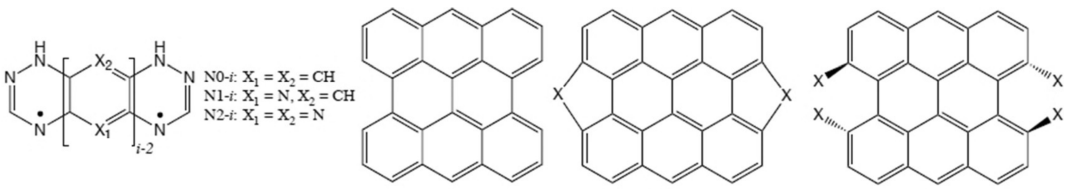

5 **6** **6**'-X X=C_2H_2, O, S **6**"-X X=F, Cl

One way to design SF chromophores is to start with a structure with too much diradical character and with $2E(T_1) < E(S_1)$, and then introduce substitutions to mitigate

the diradical character to make $2E(T_1)$ closer to $E(S_1)$. Following this route, Ito et al. designed SF chromophores with bisanthene (**6**) as a starting structure.[68] Bisanthene possesses too significant diradical character. Its calculated $E(S_1)$ and $E(T_1)$ values were 2.393 and 0.939 eV. $2E(T_1) - E(S_1) = -0.515$ indicates a substantial energy loss in SF. Ito et al. reduced the diradical character by making O, S, and C_2H_2 substitutions as in **6**'-X. The substitutions introduce two extra sextet rings to the non-diradical resonance structure and hence reduce the diradical character. The authors also substituted bisanthene with bulky halogen atoms and methyl groups as in **9**"-X to twist the structure to non-planar. The non-planarity reduces the overlap between the frontier orbitals of the two anthracene units and enlarges the HOMO–LUMO gap, reducing the diradical character. Compounds **6**'-O and **6**"-F were predicted to be promising chromophores, with $2E(T_1)$-$E(S_1) \approx 0$.

Section 1.7 Small SF Chromophores

Conventional SF chromophores such as tetracene, pentacene, and their derivatives are fairly large in size. Akdag et al. pioneered the design of small SF chromophores.[69] Small chromophores are desired because: 1) they can give high exciton density, which eventually facilitates the development of mini OPV devices ; 2) although they may not be stable, they serve as core structures for more kinetically persistent derivatives; 3) they are convenient models for theoreticians to investigate SF, like CH_2 for carbene chemistry research. The authors proposed five monocyclic structures. They are five- or six-membered aromatic rings with endocyclic electron donors (sp^2 N) and acceptors (carbonyl). Compound **7** is shown as a representative. The donors and acceptors were introduced to exert the captodative effect[70] to stabilize radical resonance structures for the

moieties that they sandwich. With a pair of such sandwiched moieties, the diradical character of **7** is enhanced. The authors calculated low-lying excitation energies for the five designed structures by using the second-order Complete Active Space Perturbation Theory (CASPT2) method with active spaces that span all π and lone pair orbitals. Such large active spaces can only be used for small molecules. Only **7** was found to satisfy Equation (2) and almost satisfy Equation (1) (close to isoergic SF), as well as $E(S_1) < E(T_2)$. Its small size should be emphasized, especially when compared with tetracene (**2**) and pentacene (**3**).

The success of the captodative strategy motivated Zeng et al. to follow the same route, but employ a special acceptor, the endocyclic sp^2 B atom.[71] The authors proposed a series of azaborine(BN)-substituted mono- and bi-cyclic aromatic structures. They calculated excitation energies of the structures by using the General Multi-Configurational Quasi-Degenerate Perturbation Theory (GMC-QDPT). Three structures (**8** to **10**) were found to be promising chromophores, and the smallest **8** is even smaller than **7**. Disregarding the methyl groups on N in **7** and recognizing the similarity between BF and CO, **7** and **8** are isoelectronic and isosteric. Through this work, the authors attempted to crosslink the two vibrant fields of singlet fission and azaborine chemistry.[72]

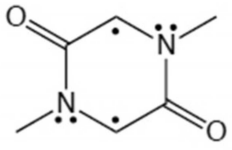

7

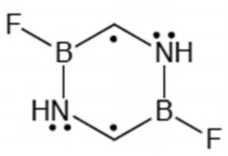

8

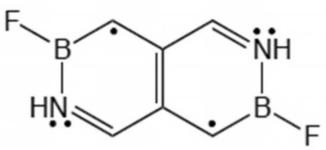

9

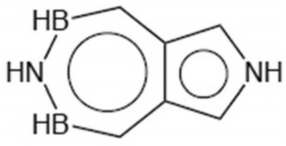

10

In Refs. [69] and [71], the two captodatively stabilized radical centers are not in contact. For instance, **8** can be viewed as being composed of two BN-substituted methyl groups, in which the C sites are not connected. Wen et al. approached the problem from another direction.[73] They started with two radical centers in contact, that is, they are covalently coupled, and then reduced the coupling and increased their diradical character by introducing donors and acceptors. The reduction in interaction is illustrated in Figure **8**, where we compare the π-bonding orbitals of the plain (upper) and a captodatively modified (lower) ethylene. The acceptor (donor) delocalizes the π singly occupied orbital of methylene through having a bonding (antibonding) interaction with the central C. The resultant smaller amplitudes at the central C atoms reduce the π–π overlap, and hence a smaller HOMO–LUMO gap is obtained.

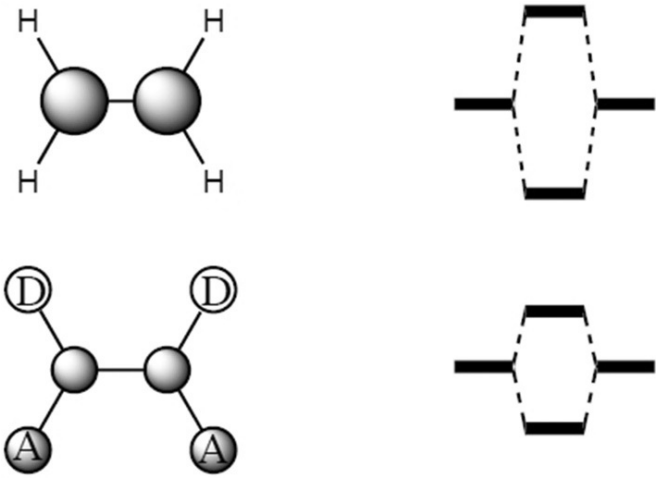

Figure 5. Weakening of the covalent interaction between two methylene radicals in forming the π bond of ethylene when they contain acceptor (A) and donor (D) substituents.

Through density functional theory (DFT) and time-dependent density functional theory (TDDFT) calculations, Bhattacharyya et al. designed a small SF chromophore based on mono-Si-substitution on anthracene (**11**).[74] Si is an electron donor and its endocyclic substitution raises the HOMO energy more than the LUMO energy. The reduced HOMO–LUMO gap increases the diradical character of **11** and makes it satisfy Equation (1), with $E(S_1)$ = 2.65 and $E(T_1)$ = 0.97 eV. The authors further introduced a CN group to **11** and the resultant structure (12) was shown to have almost isoergic SF, with $E(S_1)$-$2E(T_1)$ = 0.05 eV.

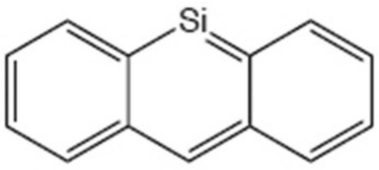

11

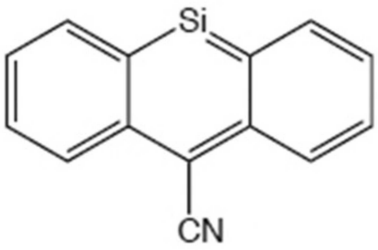

12

Section 1.8 Summary of Promising Theoretical Design

Table 1. Excitation energies (in eV) of theoretically designed promising SF chromophores.

STRUCTURE	$E(S_0)$	$E(T_1)$	$E(T_2)$
4	3.01	1.41	3.16
5 N2-4	2.60	1.08	2.75
5 N0-3	2.41	1.10	2.51
6' - O	2.80	1.36	2.92
6"- F	2.52	1.26	2.72
7	2.11	1.14	3.52
8	3.01	1.34	5.26
9	1.99	0.97	2.82
10	2.03	0.84	3.00
11	2.65	0.87	-
12	2.57	1.26	-

The calculated excitation energies of the promising SF chromophores discussed above are summarized in Table 1 for comparison. Among them, **7**, **9**, and **12** are of special interest. Their $E(T_1)$ values are close to the optimal 1 eV gap and $E(S_1)$ values are close to twice the $E(T_1)$ values, minimizing energy loss in SF. Also, the close to 2 eV S_0-to-S_1 absorption occurs at the frequency range with fairly high spectral irradiance in the solar spectrum.[75] They are high value targets for future syntheses and experimental investigations.

Section 1.9 Design of SF Chromophores with Cyclic (Alkyl)(Amino) Carbene Building Blocks, the Motivation and Objective of This Work

As introduced in the previous subsections, one obstacle for the application of the SF phenomenon in photovoltaics is that only a small number of molecules meet the three criteria of Equations (1)-(3). Among them Equations (1) and (2) are more difficult to meet. Especially, current research of SF is "overwhelmingly limited" to tetracene[7] and pentacene.[6,12,76] There is thus a strong motivation to design more SF chromophores that meet the criteria. It has been clarified that the possession of non-negligible diradical character and the lack of tetraradical character are the underlying reasons for a molecule to satisfy the two inequalities, respectively.[55,66,77,78,79] Stable molecules, either isolated in reality or optimized in silico, rarely possess significant tetraradical character. Therefore, it would be relatively easier to satisfy Eq. 2 than Eq. 1, which is thus the primary criterion for SF chromophores.

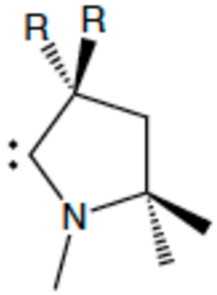

13

We have also learned that the enhancement of diradical character can be realized by introducing captodative effect.[69,73,76,80-82] These modifications shall be applied to structures that are by themselves not too low in diradical character. Otherwise, the

enhancement in diradical character may not be enough to satisfy Eq.1. Recently, attentions have been drawn to structures with cyclic (alkyl)(amino)carbenes (CAACs) as building blocks shown in **13**.[83] CAACs are persistent singlet carbenes.[84] Last year, a modular approach for connecting CAACs by spacers to form stable Kekulé diradicaloids was reported by the Bertrand group.[85] This approach allows tuning the diradical character of the CAAC-based diradicaloids through modifying the spacer, especially its length and aromaticity. Therefore, this approach opens the doorway to design CAAC-based SF chromophores. Immediately following this work, Messelberger et al. performed a computational study of a series of CAAC-spacer-CAAC dimer structures and identified several candidates as SF chromophores.[83] It is noteworthy that while CAACs are usually used as stabilizers for radical and diradical moieties attached to them,[86-90] they themselves are radical centers in those SF chromophore candidates.

Inspired by these latest advances in the field of SF, we in this work perform quantum chemistry calculations to study the possibility of designing CAAC-spacer-CAAC SF chromophores through fluorination and trifluoromethylation at the α C. The ideas of fluorination and trifluoromethylation originate from the captodative effect: by stabilizing a radical center by simultaneously attaching a donor and an acceptor to it.[91] By connecting a CAAC unit to a spacer, one electron of the carbene's σ lone pair participates in forming a σ bond with the spacer. The leftover unpaired electron occupies the π orbital of the carbene, making the carbene a π radical. The N atom adjacent to the carbene C exerts a donating effect to the singly occupied carbene π orbital. If the α C can serve as a π acceptor, or at least as a poorer π donor, the CAAC π radical unit will be stabilized by the captodative effect of the α C and the N, and the diradical character of the CAAC-

spacer-CAAC structure will be enhanced. The structure is then more likely to satisfy Eq. 1. According to the work shown below, fluorination and trifluoromethylation at the α C does enhance its π accepting capability. Only homodimers are considered in this work, since heterodimers are likely to feature more or less ionic character in their ground state, which is exclusive with diradical character.

Section 1.10 Organization of the Rest of the Thesis

In Chapter 2, details of the theoretical methods used in our study are given. In Chapter 3, the computational results are presented and discussed. The conclusions are given in Chapter 4. The introduction in Chapter 1 is included in the review article published as A. Japahuge and T. Zeng "Theoretical studies of singlet fission: searching for materials and exploring mechanisms (review)." *ChemPlusChem* **2018**, *83*, 146-182. The review article was highlighted as a Very Important Paper of the journal. The material designing study in this thesis has been published as A. Japahuge, S. Lee, C. H. Choi, and T. Zeng, "Design of Singlet Fission Chromophores with Cyclic (Alkyl)(Amino) Carbene Building Blocks." *J. Chem. Phys.* **2019**, *150*, 234306.

CHAPTER 2 METHODOLOGY

Section 2.1 MRSF-TDDFT Method for Electronic Structure Correlation

Schrödinger equation is the fundamental equation in quantum mechanics. There are two forms of the equation, the time-independent and the time-dependent Schrödinger equation. We need to solve the time-independent Schrödinger equation for the designed chromophores to obtain their excitation energies. However, it is difficult to solve Schrödinger equations for many-body systems. In practice, we rely on approximations to solve the equations. And the accuracies of the solutions are critically dependent on the approximations and whether they are applicable for the systems of interest.

Density functional theory (DFT) delivers a class of efficient methods to solve Schrödinger equations for multi-electronic systems. Traditional DFT methods are not reliable for systems whose wave functions are of multi-reference nature, i.e., that wave functions that are not dominated by one Slater determinant (or electron configuration). SF chromophores fall into this type of systems. The significant diradical character in their ground state wave functions determines the multi-reference nature of their ground state wave functions. Their excited states, with excitations out of the ground states, are also characterized by substantial contributions by several Slater determinants. In general, it is desired to develop DFT methods to handle systems with multi-reference wave functions accurately and efficiently. Such methods are especially needed for our study of designing SF chromophores.

Recently, two of our collaborators, Seunghoon Lee and Cheol Ho ChoI, developed the mixed-reference spin-flip time-dependent density functional theory (MRSF-TDDFT) formalism[92] and its analytic energy gradient. The new theory is an

improved SF-TDDFT, which can treat both dynamic and non-dynamic correlations in a balanced way. This means it can be used to study systems with multi-reference wave functions. This theory overcomes the notorious deficiencies of the conventional SF-TDDFT known as the spin-contamination problem. It is shown that MRSF-TDDFT gives improved results than those of SF-TDDFT in calculating excitation energies.[93] In the MRSF-TDDFT, the lowest triplet state obtained at the restricted open-shell DFT level is used as the reference state. The singlet and triplet response states of the same molecular structure are obtained by the linear response, i.e., one-electron transitions, from the same reference state, which is similar to configuration interaction singles.

Although the molecular orbitals of the reference states are optimized for the lowest-triplet state, the singlet and triplet response states are described by rotations from occupied orbitals to virtual orbitals of reference state. Therefore, the MRSF-TDDFT method does not bias towards the triplet response state that resembles the reference state. Geometry optimizations for all studied structures, in their ground and excited states in both singlet and triplet spin manifolds, are performed using the MRSF-TDDFT method. The method is also used for all hessian calculations.

Section 2.2 Geometry Optimization

The process of finding a settlement of a molecule where the intra-atomic forces among atoms are relatively closer to zero is called as energy minimization or geometry optimization. It is equivalent to locating stationary points on potential energy surface. As to our chromophore designs, all reported optimized dimer structures are of C_2 symmetry, unless further specified. Optimizations with C_i symmetry for several representative molecules give similar energies and structural parameters. For instance, the $(CAAC)_2$-C_2

dimer structures with C_2 and C_i symmetries have identical bond lengths at their cumulene fragments. Their calculated vertical $E(S_1)$s and $E(S_2)$s differ by only 0.002 and 0.006 eV, respectively. Hence, the discussion will be focus only on the C_2 structures. The BHHLYP functional[94,95] and the Def2-SVP basis set[96] are used in the optimization and hessian calculations, which are performed using a development version of the GAMESS-US program package.[97,98] The hessian calculations confirm that the optimized structures are true minima on potential energy surfaces. Optimization of the water dimer structure is done by the Def2-SVP and Def2-TZV PP basis sets and the BHHLYP functional. The resultant O-O distances are 2.86 and 2.90 Å, respectively. The 0.04 Å small difference corroborates the competence of the economical Def2-SVP basis set in optimizing structures with hydrogen bonding interaction. Hydrogen bonding interaction plays an important role in determining the structures of the dimers that are considered in this study. All the reported energies contain Zero Point Energy (ZPE) corrections, unless further specified. The rapid geometry relaxation associated with photoexcitation competes with SF.[1] It is hence more reasonable to use ZPE-corrected minimum-to-minimum (i.e., adiabatic) excitation energies to judge whether a molecule satisfies Eqs. 1 and 2. As shown below, structural reorganizations induced by excitation can be significant. It is well known that such excitation-induced reorganizations play an important role in energy transfer and charge transfer of organic semiconductors.[99-101] In general, significant reorganizations lead to higher barriers and lower rates of the transfers.

Section 2.3 Excitation Energy Calculations

All reported excitation energies are calculated using the second order n-electron valence state perturbation theory (NEVPT2) method[102,103] implemented in the ORCA

program package,[104] to account for the dynamic correlation effect with the Def2-TZVPP basis set.[96] Full π valence active spaces are used in the NEVPT2 calculations. Please note that the exclusion of the N lone pair orbitals from the active space overestimates the vertical $E(S_1)$ of the $(CAAC)_2$-C_2 dimer by 0.32 eV in a test calculation. It is thus necessary to include them, i.e., to use the full π valence active space. The NEVPT2 wave functions are consistent with those obtained in the MRSF-TDDFT calculations. Therefore, the geometry optimizations and excitation energy calculations are performed for the same set of states.

In the NEVPT2 calculations, states that are relevant in an excitation are averaged equally. For instance, to calculate adiabatic $E(S_1)$ of a molecule, NEVPT2 calculations weighting S_0 and S_1 equally are carried out at S_0- and S_1-optimized structures. The difference between $E(S_1)$ at S_1 structure and $E(S_0)$ at S_0 structure (abbreviated as $E(S_0)@S_0g$ and $E(S_1)@S_1g$), offset by the ZPEs of the respective structures, gives the adiabatic $E(S_1)$. We gradually include more states in the average to ensure that proper states have been captured by the minimum average scheme. If not, then more states are included until convergences of the energies and wave functions of the interesting states are attained. To calculate an adiabatic excitation energy, we always average the same number of states in the NEVPT2 calculations at the two optimized structures.

The CAAC model adopted in this work is shown in structure **13**, with all substituents on the 5-membered ring being methyls. The two R groups at the α C atom are to be replaced by F atoms and trifluoromethyls to tune the electron-accepting capacity of the α C. The resultant CAAC structures are accordingly labelled as CAAC(F) and CAAC(TFM).

CHAPTER 3 CALCULATION AND DISCUSSION

Section 3.1 The Fluorination and Trifluoromethylation

The HOMO and LUMO of CAAC in its S_0 state are shown in Figure 6(a) and (b). With the N as a π donor, the π LUMO features antibonding character between the N atom and the carbene C atom, and its energy is raised. With the lone pair electrons occupying the σ HOMO, CAAC is a typical σ donating N-heterocyclic carbene (NHC). In the CAAC π LUMO, there is almost no bonding or antibonding interaction between the carbene C atom and the α C atom. Quantitatively, the π LUMO contributes -0.001 Mayer bond order[105] between the two atoms. Once we replace the two methyls attached to the α C by F atoms, the C-F σ^* antibonding orbitals have lower energy and are more localized on the α C. The σ^* orbitals will then become more effective in overlapping with the p_π AO on the carbene C. For comparison, the π LUMO contributes 0.091 Mayer bond order between the two C atoms in CAAC(F). This typical through-bond bonding interaction[106] lowers the energy of the π LUMO and stabilizes the radical with the unpaired electron in the π orbital.

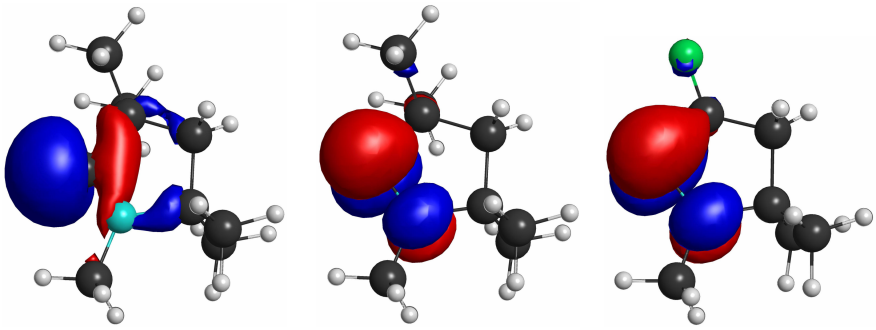

(a) (b) (c)

Figure 6. (a) and (b) the σ HOMO and π LUMO of CAAC in its singlet ground state; (c) the π LUMO of CAAC (F).

The comparison of Figure 6(b) and (c) clearly shows that with the more electronegative F atoms, the π LUMO features some bonding interaction between the carbene C and the α C. As a reflection of the stabilization of the π LUMO, the vertical E(T_1) of CAAC(F) is calculated to be lower than that of CAAC by 0.11 eV (2.61 vs. 2.72 eV), and the T_1 state has one electron in each of the σ and the π orbital. CAAC(TFM) is in between the other two structures. The π LUMO contributes 0.012 Mayer bond order between the carbene C atom and the α C atom in CAAC(TFM), and the vertical E(T_1) is 2.67 eV. The BHHLYP HOMO-LUMO gaps are 4.57, 4.55, and 4.47 eV for CAAC, CAAC(TFM), and CAAC(F). The gap decrease is consistent with the decrease of the vertical E(T_1) and the increase of the Mayer π bond order between the carbene C atom and the α C atom. We are aware that according to the σ electron donor-acceptor indicator proposed by Oziminski et al., CF_3 is less electronegative than CH_3.[107] With no intention to question the validity of this useful indicator, we here just present a trend that is in line with the chemical intuition: the presence of the F atoms in CF_3 makes it more electronegative than CH_3, and the α C atom with the two CF_3 groups exhibits a stronger π accepting capability. The inconsistence is partially attributed to the complexity in defining electronegativity,[108] especially electronegativity of functional groups.[109]

There are other ways to stabilize the π LUMO of a carbene. One straightforward way is to put a π acceptor, e.g., a tertiary B atom, beside the carbene C. We here adopt the fluorination and trifluoromethylation strategies, with the purpose to minimize the modification of the CAAC structure. It is of critical importance to keep a quaternary C in the α position, which provides steric protection and enhances the stability of CAACs.[84]

The results presented in this work show that it is possible to stabilize the π LUMO while maintaining a quaternary α C. While we are focusing on attaching electronegative substituents onto the α C, another way to enhance the diradical character is to attach electropositive substituent onto the N. This substitution strategy forms a subject for future research.

Section 3.2 CAAC Dimers with a C_2 Spacer

We first examine the dimers of the three types of CAAC units connected by a C_2 spacer. The dimers are called $(CAAC)_2$-C_2, $(CAAC(TFM))_2$-C_2, and $(CAAC(F))_2$-C_2, respectively. These structures are of special interest as the $(CAAC)_2$-C_2 cumulene has been isolated in good yield.[110,111] It is thus desirable to investigate the (F) and (TFM) analogues with the same skeleton. We believe that the knowledge accumulated in synthesizing $(CAAC)_2$-C_2 is helpful in synthesizing the analogues. Please note that each of the CAAC dimers is examined as a singlet fission chromophore. We need two of the CAAC dimers to give the chromophore dimer model in Figure 2.

The optimized structures of the S_0, T_1, and S_1 states of $(CAAC)_2$-C_2 are shown in Figure 7(a)-(c) and the calculated results are summarized in Table 2. The 172° dihedral angle d_{NCCN} indicates a cumulene resonance structure for this molecule. The occupancy of the lowest unoccupied natural orbital (n_{LUNO}) is 0.13, which indicates the diradical character of this molecule.[112] The n_{LUNO} mainly arises from the configuration with the HOMO-to-LUMO two-electron excitation configuration. The orbitals are shown in Figure 7(d) and (e). This excitation corresponds to polarizing the distributions of the two electrons in HOMO, so that when one electron occupies the π orbital of one carbene, the

other occupies the π orbital of the other carbene. This suggests an increase of diradical character with the π radical centers on the carbene C atoms. Meanwhile, the out-of-plane π bonding orbital between the two central C atoms is strengthened due to the corresponding (anti)bonding character in the LUMO (HOMO). Therefore, the S_0 state adopts the additional diradical resonance structure shown in Figure 7(h). In consistence with the diradical resonance structure, the central CC bond of the cumulene moiety is shorter than the other two (1.26 vs. 1.33 Å). Please note that these calculated bond lengths are in excellent agreement with the experimental values of 1.27 and 1.33 Å.[110] The XRD-determined bond lengths are for the single crystal of $(CAAC)_2$-C_2 with diisopropylphenyls (Dipp) attached to the N atoms. The agreement reflects the accuracy of the MRSF-TDDFT structure optimization and the appropriateness of replacing the Dipp groups by methyls.

The T_1 state corresponds to the HOMO-to-LUMO single electron excitation, resulting in the pure diradical resonance structure shown in Figure 7(i). The resonance structure is consistent with the T_1 geometrical structure: the 1.24 Å short CC triple bond in the center and the almost perpendicular dihedral angle made by the two CAAC fragments ($d_{\mathrm{NCCN}} = 97°$). The ZPE-corrected vertical and adiabatic $E(T_1)$s are calculated to be 2.53 and 1.52 eV, respectively. The 1.01 eV large reorganization energy is consistent with the significant structural change between the S_0 and T_1 states.

Table 2. Calculated results for the three C2-connected dimers. All energies are given in eV.

	CAAC	(TFM)	(F)
Adiabatic $E(S_1)$	2.15	2.47	2.33
Vertical $E(S_1)$ (f)	3.71 (0.002)	3.66 (0.003)	3.71 (0.004)
Adiabatic $E(S_2)$[a]	3.50	3.36	3.30
Vertical $E(S_2)$ (f)	3.71 (0.76)	3.55 (0.75)	3.53[b] (0.75)
Adiabatic $E(T_1)$	1.52	1.43	1.29
Vertical $E(T_1)$	2.53	2.33	2.19
n^c_{LUNO}	0.13	0.14	0.15
$\Delta E^{(1)}_{SF}$	-0.89	-0.39	-0.25

[a] The S_2 structural optimizations and ZPE calculations are carried out with C_i symmetry, in which the S_2 and S_1 states belong to different irreducible representations. Therefore, S_1-S_2 root flipping does not occur in the course of S_2 optimizations; [b] for the (F) dimer, this is actually the vertical $E(S_1)$. We use S_2 to label this state for comparing its energy with the energies of the truly vertical S_2 states with the same HOMO-to-LUMO excitation scheme in the CAAC dimer and the (TFM) dimer; [c] calculated at S_0 structure.

The S_1 state arises from the single electron HOMO-to-LUMO+1 excitation. The planar framework remains in the S_1 optimized structure, with d_{NCCN} = 175° . At the BHHLYP/Def2-SVP level, the HOMO-LUMO gap is calculated to be 3.51 eV, not significantly lower than the 3.91 eV HOMO-LUMO+1 gap. Please note that the orbital energies are obtained in a restricted open-shell BHHLYP calculation for the lowest quintet state at the S_0 structure, which treats HOMO-1 to LUMO+1 equally. Their orbital energies are hence comparable. The HOMO and LUMO are compact and they are both

out-of-plane π orbitals. They hence have a substantial spatial overlap, which results in a large exchange integral that gives a high singlet excited state with one electron in each orbital. Please note that the large orbital overlap favors a low-lying triplet state. On the contrary, the HOMO and LUMO+1 (Figure 7(f)) are perpendicular and have a smaller exchange integral that can offset their 0.4 eV orbital gap. Consequently, the HOMO-to-LUMO+1 singlet excitation is of lower energy, while the HOMO-to-LUMO excitation gives the S_2 state. The vertical excitation energies of the two singlet states are close. With ZPE corrections, they are both 3.71 eV.

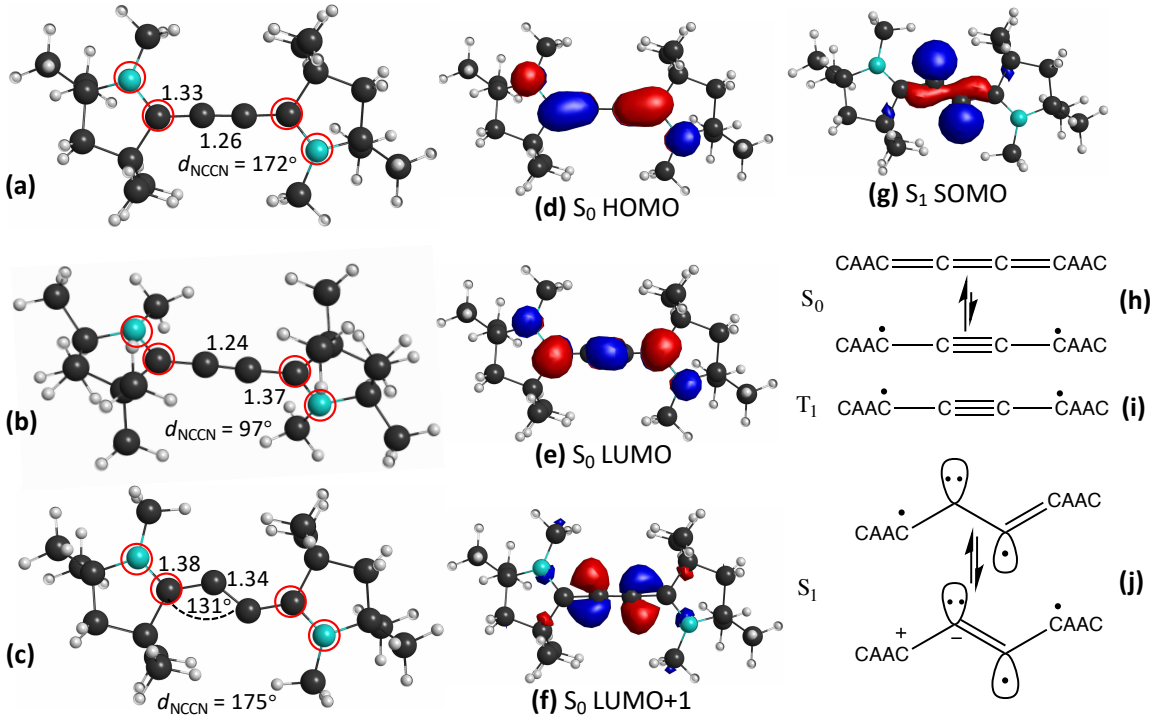

Figure 7. The optimized structures of the (a) S_0, (b) T_1, and (c) S_1 states of $(CAAC)_2$-C_2; (d)-(g) frontier orbitals of the structures of the denoted states; (h)-(i) typical resonance structures of the three states. Some important structural parameters are shown in panels (a)-(c), where the bond lengths are given in Å and the four atoms that define the dihedral angles are highlighted by red circles. In panel (i), only one set of resonance structures are shown for the S_1 state. There is another set which includes the symmetry images of the shown structures.

We cannot reproduce the non-ZPE-corrected 2.88 eV vertical $E(S_1)$ of $(CAAC)_2$-C_2 reported in Ref. 83. We took the structure from the Supportive Information of the paper and averaged the lowest five singlet states (employing the same state average scheme in the reference) in performing NEVPT2 calculation for the structure. The vertical $E(S_1)$ is calculated to be 3.13 eV, with $f = 0.58$. This f is close to the 0.6 reported in Ref. 83. This S_1 state corresponds to the HOMO-to-LUMO excitation. The HOMO-to-LUMO+1 excitation gives the S_2 state, with the non-ZPE-corrected vertical $E(S_1) = 3.60$ eV. There are two factors that contribute to the differences between the results in Ref. 83 and ours. (1) Different active spaces are used. A smaller 4 electrons in 4 orbitals active space was used in Ref. 83, while the full valence π active space with 8 orbitals and 10 electrons are employed in the present work. As mentioned in Chapter 2, the calculated excitation energies of the C_2-connected dimers (and the C_4-connected dimers too) are highly sensitive to the active space, varying by tenths of eV. (2) Different dimer structures were used. The 1.33 and 1.26 Å CC bond lengths demonstrated in Figure 7(a) are in good agreement with the experimental values. The corresponding bond lengths of the structure used in Ref. 83 are 1.44 and 1.18 Å.

The S_1-optimized structure features an in-plane bending of the cumulene moiety, resulting in the 131° ∠CCC shown in Figure 7(c). The in-plane π^* antibonding LUMO+1 at the S_0 structure has evolved to the nonbonding singly occupied molecular orbital (SOMO) at the S_1 structure (Figure 7(g)). Correspondingly, the in-plane π bonding orbital has also evolved to a similar nonbonding orbital. There is thus little in-plane π bonding interaction between the two central C atoms. The S_1 state adopts the resonance structures

shown in Figure 7(j), with three electrons distributed in the two in-plane sp^2 hybridized non-bonding orbitals. The ZPE-corrected vertical and adiabatic $E(S_1)$s are calculated to be 3.71 and 2.15 eV. The significant structural change in the S_1 state is commensurate with the 1.56 eV large reorganization energy. The perpendicular HOMO and LUMO+1 give the 0.002 small oscillator strength (f) for the vertical S_0-to-S_1 excitation. The 2.15 eV adiabatic $E(S_1)$ and the 3.71 eV vertical $E(S_1)$ are in fair agreement with the UV/Vis spectrum of the dimer in CH_2Cl_2 solution.[111] The spectrum consists of a structureless band, whose low energy edge is at 2.32 eV (535 nm) and with very low intensity. The intensity of the band increases sharply as the absorption energy increases to 3.65 eV (340 nm), beyond which the absorption was not recorded. The 340 nm absorption is so intense that it must involve the excitation to S_2, whose adiabatic and vertical excitation energies are 3.50 and 3.71 eV (354 and 334 nm), respectively, and f = 0.76. Please note that the agreement between the calculated excitation energies and the UV/Vis spectrum corroborates the accuracy of our calculation methods.

With the C_i symmetry of the dimer in crystal,[111,110] the HOMO-to-LUMO+1 excitation to the S_1 state is symmetry forbidden. In solution, the dimer can also adopt C_2 symmetry, as the C_2 configuration is only higher by 0.002 eV (estimated at the NEVPT2 level) than the C_i configuration. Although the transition is now not symmetry-forbidden, as mentioned above, the small f = 0.002 arises from the transition between two perpendicular π orbitals. Despite the small (strictly zero) oscillator strength in C_2 (C_i) symmetry, the transition may be turned on by vibrations, and one possible vibrational mode is the torsional motion of the CAAC units about the C_2 spacer. Such an out-of-plane vibration can induce mixing of the out-of-plane LUMO and the in-plane LUMO+1,

and hence turns on the HOMO-to-LUMO+1 transition. According to our MRSF-TDDFT calculation, the frequency of this mode is only 40 cm^{-1} low. Out-of-plane wagging and rocking modes of the CAAC units with respect to the spacer are of similarly low frequencies. These vibrations can be thermally activated. Overall, the structure of the dimer is not rigid and vibration-induced S_0-to-S_1 transition is possible. Other than the symmetry-breaking vibrations, the S_0-to-S_1 transition intensity may also be enhanced by the surrounding CH_2Cl_2 polar solvent molecules. The mixing of the perpendicular LUMO and LUMO+1 can be induced by an electric dipole pointing in a direction between them. The conjecture of the vibration- and solvent-induced S_0-to-S_1 transition is consistent with the low intensity of the absorption at 2.32 eV (535 nm).

The excited states of $(CAAC(TFM))_2$-C_2 and $(CAAC(F))_2$-C_2 feature similar excitation schemes and take similar resonance and geometrical structures for those states. Their higher diradical characters are reflected by their lower vertical $E(T_1)$s of 2.33 and 2.19 eV and their larger n_{LUNO}s of 0.14 and 0.15. The order of the diradical character follows the expectation based on the stabilization of the CAAC π LUMO by the trifluoromethylation and fluorination at the α C. With structural reorganization, the adiabatic $E(T_1)$s are calculated to be 1.43 and 1.29 eV.

The S_1 state has little to do with the diradical character, and the ZPE-corrected vertical $E(S_1)$s of the (TFM) and (F) dimers are calculated to be 3.66 and 3.71 eV, which are close to the 3.71 eV of the unsubstituted structure. After the S_1 structures are optimized, the adiabatic $E(S_1)$s are 2.47 and 2.33 eV, larger than the 2.15 eV of the unsubstituted structure. The higher $E(S_1)$s leave more room for the substituted dimers to satisfy Eq. 1. Please note that at the S_0 structure of the (F) dimer, the HOMO-to-

LUMO+1 excitation requires slightly higher energy than the HOMO-to-LUMO excitation (3.71 vs. 3.53 eV, also see the *b* note in Table 2). The HOMO-to-LUMO+1 excited state becomes lower in energy in the course of the S_1 structural optimization and gives the adiabatic S_1 state. For this reason and also the convenience to compare with the results of (CAAC)-C_2 and the (TFM) dimer, we still label the HOMO-to-LUMO+1 excitation at the S_0 structure the S_1 state, while the HOMO-to-LUMO excitation the S_2 state.

With the ZPE-corrected adiabatic energies, $\Delta E_{SF}^{(1)} = E(S_1) - 2E(T_1)$ = -0.89, -0.39, and -0.25 eV for $(CAAC)_2$-C_2, the (TFM), and the (F) dimers. None of them meets the primary criterion Eq. 1 for SF chromophores, although the trend is in the right direction with the TFM and F substitutions. In addition to the energy mismatches, these molecules have another disadvantage as SF chromophores. Their > 3.6 eV vertical $E(S_1)$s are in the UV region, in which the solar spectrum has low photon flux density. And the S_1 states have negligible oscillator strengths. The S_2 states involve the HOMO-to-LUMO excitation and their oscillator strengths are more substantial. Their vertical excitation energies are deeper in the UV region (except for the (F) dimer, whose vertical $E(S_2)$ is at the border of the UV and Vis regions). Overall, the three CAAC dimers do not have good absorption of the solar spectrum. The importance of structural reorganization of the excited states is clearly shown in this series of calculations. If we compare the vertical $E(S_1)$s and the adiabatic $E(T_1)$s, all three molecules satisfy Eq. 1. The > 1.19 eV large reorganization energies of the S_1 states, however, reverse the signs of the respective $\Delta E_{SF}^{(1)}$s.

Section 3.3 CAAC Dimers with a C_4 Spacer

The HOMO and LUMO in Figure 7(d) and (e) show that the π LUMOs of the CAAC units have (anti)bonding interactions with the LUMO (HOMO) of the C_2 spacer. Without these interactions, each of the CAAC π LUMO would hold an unpaired electron in the dimer, and the dimer would be a pure diradical. The bonding and antibonding interactions open up the HOMO-LUMO gap and reduce the diradical character, so that the dimer does not satisfy Eq. 1. A longer spacer, with its attenuated HOMO and LUMO amplitudes at the connecting sites with the CAAC units, is likely to reduce the bonding/antibonding interactions and increase the diradical character, making the dimer satisfy Eq. 1. Following this logic, we increase the length of the spacer from C_2 to C_4. The calculated results of the C_4-connected dimers are summarized in Table 3.

The S_0, T_1, and S_1 structures of $(CAAC)_2$-C_4 are shown in Figure 8(a)-(c), which share geometrical features with the C_2 analogues. This is reasonable given the similarity in electronic structure of cumulenes with different lengths. While the HOMO in Figure 8(d) shows bonding interaction between the CAAC fragments and the spacer, the LUMO+1 in Figure 8(f), which corresponds to the LUMO in Figure 7(e), shows largely nonbonding character. The LUMO and LUMO+1 are almost degenerate, with the 2.53 and 2.62 eV HOMO-LUMO and HOMO-LUMO+1 gaps at the BHHLYP level of calculation.

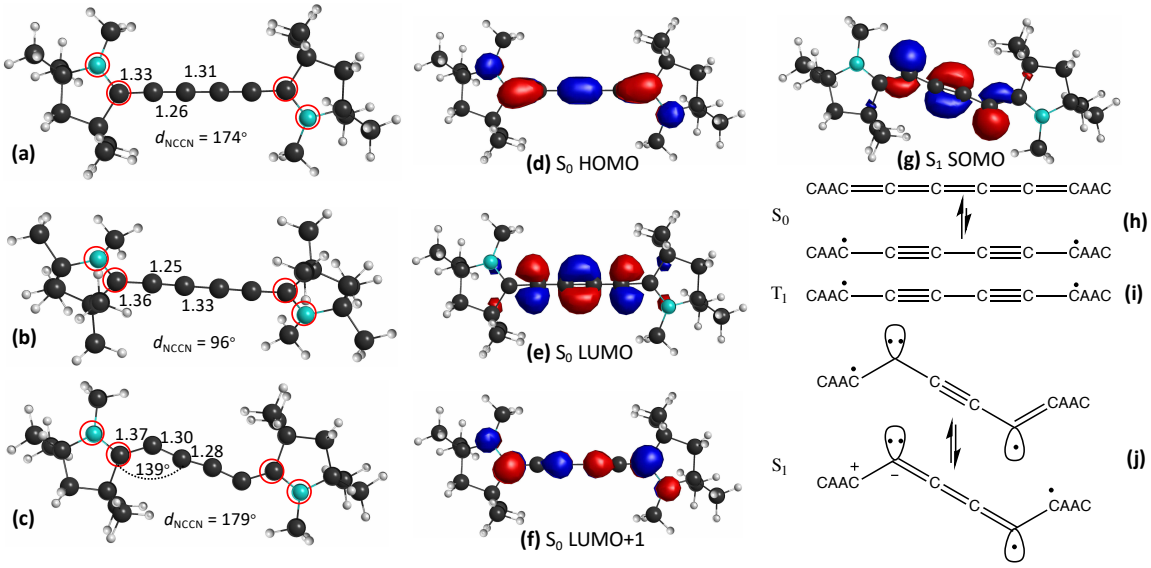

Figure 8. The optimized structures of the (a) S_0, (b) T_1, and (c) S_1 states of $(CAAC)_2$-C_4; (d)-(g) frontier orbitals of the structures of the denoted states; (h)-(j) typical resonance structures of the three states. Some important structural parameters are shown in panels (a)-(c), where the bond lengths are given in Å and the four atoms that define the dihedral angles are highlighted by red circles. In panel (j), only one set of resonance structures are shown for the S_1 state. There is another set which includes the symmetry images of the shown structures.

The T_1 and S_1 states involve the same excitations as in the C_2-connected dimers, except that the LUMO and LUMO+1 of the C_4-connected dimer correspond to the LUMO+1 and LUMO of the C_2 analogue. The vertical $E(T_1)$s are 1.80, 1.65, and 1.58 eV for $(CAAC)_2$-C_4, $(CAAC(TFM))_2$-C_4, and $(CAAC(F))_2$-C_4, respectively, and the ground state n_{LUNO}s are 0.19, 0.20, and 0.21. Both sets of data indicate the stronger diradical characters brought by the C_4 spacer, and brought by the trifluoromethylation and fluorination. The pure diradical character of the T_1 state results in the structural reorganization to the perpendicular arrangement of the CAAC fragments as shown in Figure 8(b), along with a 0.74 eV substantial reorganization energy.

In the S_1 state the antibonding LUMO is occupied and evolves to the SOMO at the S_1 structure (Figure 8(g)) following the bending of the C_6 cumulene fragment. The SOMO exhibits nonbonding character at the two ends of the spacer. The 0.79 eV S_1 reorganization energy is similar to the T_1 analogue. The structures, orbitals, and excitation schemes of the C_4-connected dimers are similar to those of the C_2-connected dimers. We thus assign the similar resonance structures as shown in Figure 8(h)-(j) to the three states of $(CAAC)_2$-C_4. The structures and orbitals of the (TFM) and (F) dimers are similar to those of the unsubstituted dimer and are hence not shown in Figure 8.

Table 3. Calculated results for the three C4-connected dimers. All energies are given in eV.

	CAAC	(TFM)	(F)
Adiabatic $E(S_1)$	1.65	1.89	1.87
Vertical $E(S_1)$ (f)	2.44 (0.0001)	2.50 (0.001)	2.56 (0.001)
Vertical $E(S_2)^a$ (f)	3.33 (0.71)	3.19 (0.61)	3.16 (0.62)
Adiabatic $E(T_1)$	1.06	0.98	0.91
Vertical $E(T_1)$	1.80	1.65	1.58
$E(T_1)@S_1g$	1.40	1.82	1.65
n^b_{LUNO}	0.19	0.20	0.21
λ^c	1.08	1.51	1.41
Barrier^d	0.56	0.41	0.33
$\Delta \mathrm{E}^{(1)}_{\mathrm{SF}}$	-0.47	-0.07	0.05

^{a} Without ZPE correction; ^{b} calculated at S_0 structure; ^{c} reorganization energies for $S_0S_1 \rightarrow T_1T_1$; ^{d} barrier for $S_0S_1 \rightarrow T_1T_1$.

The S_1 and T_1 energies of the three C_4-connected dimers, both vertical and adiabatic, are lower than the C_2 counterparts. This is consistent with the smaller HOMO-to-LUMO and HOMO-to-LUMO+1 gaps brought by the longer length of the molecules. With the adiabatic $E(S_1)$s and $E(T_1)$s, $\Delta E^{(1)}_{SF}$= -0.47, -0.07, and 0.05 eV. The (TFM) dimer is close to satisfy and the (F) dimer satisfies Eq. 1. The 0.07 eV SF endoergicity of the (TFM) dimer can be overcome by thermal activation. Even for the unsubstituted structure, the subtraction results in a less negative value than the C_2 analogue. With the

smaller orbital gaps, the vertical excitation energies of the lowest light-absorbing singlet excited state $E(S_2)$s are 3.33, 3.19, and 3.16 eV for the three C_4-connected dimers, all smaller than the corresponding energies of the C_2-connected dimers. The S_2 state is dominated by the HOMO-to-LUMO+1 single electron excitation and has large oscillator strength: f = 0.71, 0.61, and 0.62 for the three dimers. Those absorptions occur in the visible region of the solar spectrum, which has higher photon flux density than the UV region for the C_2-connected dimers. The $E(S_2)$s above do not contain ZPE corrections. They are higher than the corresponding $E(S_1)$s by 0.5 eV, and the ZPE corrections would not alter the S_1-S_2 energy ordering. We hence do not optimize the S_2 structures and calculate their ZPEs. On the contrary, the vertical $E(S_1)$ and $E(S_2)$s of the C_2-connected dimers are close and it is necessary to include ZPE corrections to clarify the energy ordering.

Overall, the improvement by replacing the C_2 spacer by the C_4 is evident. However, it is too early to conclude that $(CAAC(TFM))_2$-C_4 and $(CAAC(F))_2$-C_4 are good candidates for SF chromophores. The substantial structural reorganizations in the S_0-to-S_1 and S_0-to-T_1 excitations and the significant structural differences between the S_1- and T_1-optimized structures imply large reorganization energies (λs) for the $S_0S_1 \rightarrow T_1T_1$ processes in the two dimers. λ can be approximated as

$$\begin{aligned}\lambda &= E(T_1)@S_0g + E(T_1)@S_1g - 2E(T_1)@T_1g \\ &= E(T_1)@S_0g + E(T_1)@S_1g - E(S_1)@S_1g + \Delta E_{SF}^{(1)}. \end{aligned} \quad (4)$$

Please note that $E(S_0)@S_0g$ has been defined to be the 0 reference. For the C_4-connected dimers, the T_1 states at the S_1 structures have the same occupation scheme as the corresponding S_1 states. The different T_1 occupation schemes compared to those in the

S_0 structures are a reasonable result of the stabilization of the S_1 SOMO shown in Figure 8(g). With the excitation energies reported in Table 3, is calculated to be 1.08, 1.51 and 1.41 eV for the three C_4-connected dimers. According to the Marcus Theory[113], the barrier for the fission can be estimated as $\frac{\left(\lambda-\Delta E_{SF}^{(1)}\right)^2}{4\lambda}$. For the three dimers, the barriers are estimated to be 0.56, 0.41 and 0.33 eV, respectively. They are fairly high for a photo-induced process such as SF, recalling the limited life times of the S_1 states. Although the (TFM) and (F) dimers satisfy the thermodynamics criterion Eq. 1, SFs are not likely to occur in those systems due to kinetics unfavorability. Please note that only the Marcus Theory is used to estimate the SF barriers in this work, without any intention to claim that the fissions, if they occur, follow the perturbation mechanism of the theory. It requires excited states dynamics simulations to explore the time scales of singlet fission in those chromophore candidates. And these simulations are beyond the scope of this research. Therefore, we cannot conclude on the validity of the Marcus Theory in the possible SF of the chromophore candidates studied in this work.

The large barriers arise from the significant structural reorganizations in the T_1 states from the S_0 and S_1 structures to the T_1 structure. The C_2 and C_4 spacers are cylindrically symmetric, and so are their valence π systems. The cylindrical π systems allow the two CAAC units to take a perpendicular configuration along the spacers, so that the SOMOs of the T_1 states are perpendicular to each other and change from bonding and antibonding orbitals in the S_0 structure to nonbonding orbitals in the T_1 structure (Figure 9).

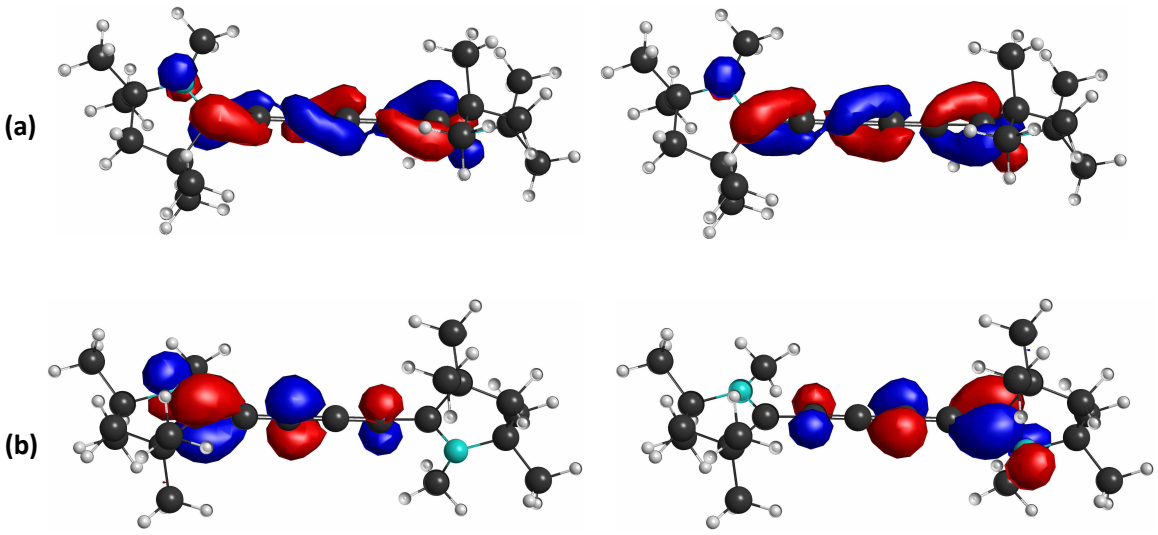

Figure 9. (a) The two singly occupied molecular orbitals $SOMO_1$ and $SOMO_2$ in the T_1 state of $(CAAC)_2$-C_4 and (b) the corresponding localized orbitals obtained from $1/\sqrt{2}(SOMO_1 \pm SOMO_2)$, which are perpendicular π orbitals.

Our calculation shows that each of the SOMOs in Figure 9(a) contributes ≤ 0.06 Mayer bond order between adjacent C atoms along the central linear fragment of the molecule. The nonbonding nature of the SOMOs is evident. These nonbonding SOMOs lower $E(T_1)$ along the coplanar-to-perpendicular structural reorganization, just as in the case of the triplet ethylene. Please note that by "coplanar" and "perpendicular", we only consider the configuration of the N, the carbene C, and the α C in the two CAAC units, and the spacer. The significant T_1 structural reorganization has two opposite effects for $(CAAC(TFM))_2$-C_4 and $(CAAC(F))_2$-C_4 : (1) it lowers their adiabatic $E(T_1)$s so that Eq. 1 is satisfied or closed to be satisfied; (2) it raises the reorganization energies and also the barriers in SF, so that the two dimers are unlikely to undergo SF. The cylindrical π systems consist of perpendicular (out-of-plane and in-plane) π orbitals in the S_0 structures. The S_1 states arise from electron transition from out-of-plane orbital to in-plane orbital. The antibonding interaction of the singly occupied in-plane π^* orbital is

mitigated by the in-plane bending of the S_1 structure, which enhances the nonbonding character of the orbital. In short, the cylindrical π systems of the C_2 and C_4 spacers are responsible for their large S_1 and T_1 reorganization energies.

Knowing the kinetics unfavorability, we do not need to consider Eq. 2 for the C_4-connected dimers. we mention in passing that the optimizations of T_2 structures of the C_2- and C_4- connected dimers failed to converge. This is because the T_2 states have the same ^3B symmetry as the T_1 states and the two states exchange their characters (i.e., root flipping) during the optimization. The T_2 states of the C_2-connected dimers correspond to the HOMO-to-LUMO+1 excitation, and C_4 analogues correspond to the HOMO-1-to-LUMO excitation. The HOMO-1 of $(CAAC)_2$-C_4 is shown in

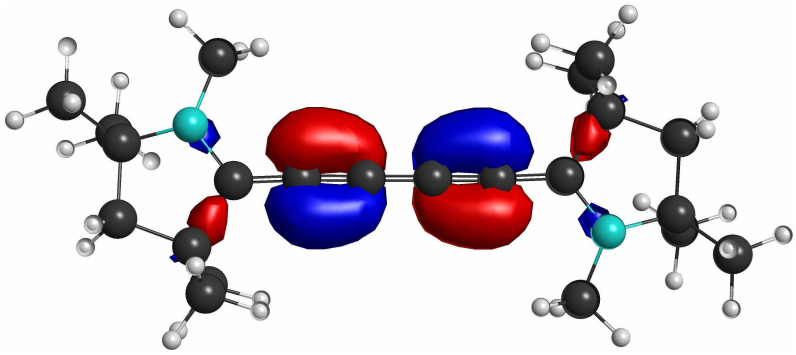

Figure 10. HOMO-1 of $(CAAC)_2$-C_4.

Section 3.4 CAAC Dimers with a *Para*-Phenylene Spacer

To avoid the problem induced by the cylindrical system of the spacer, we select the *p*-phenylene (abbreviated as Ph) as the spacer to connect two CAAC moieties. Unlike the sequence of presentation in the previous sections, we first focus on the results of $(CAAC(F))_2$-Ph and $(CAAC(TFM))_2$-Ph. This is because the optimization of the S_1 state of $(CAAC)_2$-Ph failed.

The S_0-, T_1-, and S_1-optimized structures of $(CAAC(F))_2$-Ph are shown in Figure 11(a), (b), and (c). The calculated results are summarized in Table 4. They look more similar to each other than the C_2 and C_4 analogues. Especially, the key dihedral angle changes by up to 20° only. Here, we choose the dihedral angle made by the CAAC unit and the phenyl spacer (d_{NCCC}) to indicate the coplanarity of the central fragment of the dimer. The smaller changes in the structure are consistent with the smaller S_1 and T_1 reorganization energies, which are 0.20 and 0.54 eV, respectively, vs. the 0.69 and 0.67 eV of $(CAAC(F))_2$-C_4. The (TFM) dimer shares similar structures with $(CAAC(F))_2$-Ph and thus also has smaller S_1 and T_1 reorganization energies than its C_4 counterpart. The replacement of C_4 by *p*-phenylene does point in the right direction.

The 1.53 eV vertical $E(T_1)$ of $(CAAC(F))_2$-Ph is similar to the 1.58 eV of $(CAAC(F))_2$-C_4. This suggests similar diradical characters of the two dimers. The 0.18 n_{LUNO} of $(CAAC(F))_2$-Ph, however, suggests a lower diradical character. This inconsistence is attributed to the difference in the active spaces in use. For $(CAAC(F))_2$-C_4, the in-plane π electrons can be excited and contribute to the higher 0.21 n_{LUNO}. Similar in-plane π electrons are not present in $(CAAC)_2$-Ph. It is more reasonable to compare n_{LUNO}s from calculations with comparable active spaces, e.g., those of the C_2-

and C_4-connected dimers. We hence take the vertical $E(T_1)$ as a more reliable indicator to compare the diradical characters of $(CAAC(F))_2$-Ph and $(CAAC(F))_2$-C_4.

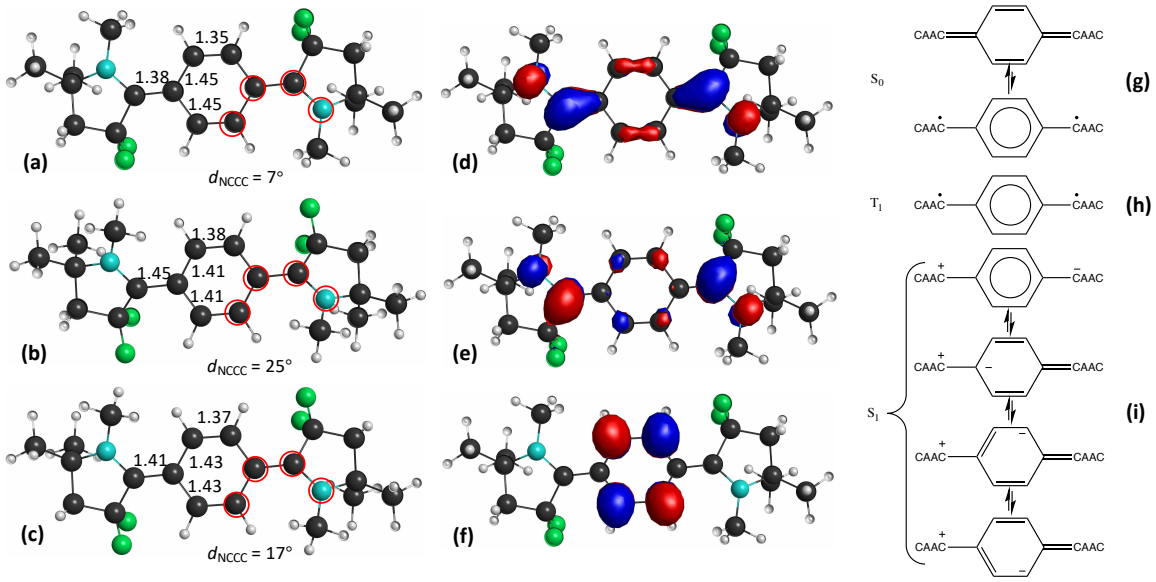

Figure 11. The optimized structures of the (a) S_0, (b) T_1, and (c) S_1 states of $(CAAC(F))_2$-Ph; (d)-(f) frontier orbitals of the structures of the S_0 state; (g)-(i) typical resonance structures of the three states. Some important structural parameters are shown in panels (a)-(c), where the bond lengths are given in Å and the four atoms that define the dihedral angles are highlighted by red circles. In panel (i), only some resonance structures are shown for the S_1 state. The others include those with the + and - charges being swapped and those with the symmetry images.

$(CAAC(F))_2$-Ph satisfies Eq. 1, with $\Delta E_{SF}^{(1)} = -0.62$ eV. Both the S_1 and T_1 states correspond to the HOMO-to-LUMO excitation, and the HOMO and LUMO are shown in Figure 11(d) and (e). The HOMO (LUMO) arises from (anti)bonding interaction between the LUMO (HOMO) of the phenylene spacer and the two π orbitals of the carbenes. $(CAAC(F))_2$-Ph bears a typical *p*-quinodimethane core structure, and its diradical character is associated to the S_0 resonance structure with an aromatic phenylene (see the S_0 resonance structures in Figure 11(g)). The S_0 state is dominated by the resonance

structure with alternating CC single and double bonds, as reflected by the bond lengths shown in Figure 11(a). The T_1 state simply takes the diradical resonance structure associated with the phenylene spacer in its aromatic form. Correspondingly, the CC bond lengths of the phenylene are more equalized in this state, and the CC bonds that connect the CAAC units and the spacer are elongated from 1.38 to 1.45 Å (i.e., from double bonds between sp^2 C atoms to single bonds).

Table 4. Calculated results for the two substituted Ph-connected dimers. All energies are given in eV

	CAAC	(TFM)	(F)
Adiabatic $E(S_1)$	2.45[a]	2.31	2.60
Vertical $E(S_1)$ (f)	2.59 (0.83)	2.45 (0.70)	2.70 (0.85)
Adiabatic $E(T_1)$	1.24[a]	0.94	0.99
Vertical $E(T_1)$	1.63	1.41	1.53
$E(T_1)@S_1g$	1.34[a]	1.13	1.20
Adiabatic $E(T_2)$	2.68	3.18	3.07
n^b_{LUNO}	0.16	0.20	0.18
λ^c	0.49	0.66	0.75
Barrier[d]	0.14	0.02	0.02
$\Delta E^{(1)}_{SF}$	0.03	0.43	0.62
$\Delta E^{(2)}_{SF}$	0.20	1.30	1.09

[a] The adiabatic $E(S_1)$ and $E(T_1)@S_1g$ of the CAAC dimer is for the S_1-optimized structure with C_2 symmetry, which has an imaginary frequency. [b] calculated at S_0 structure; [c] reorganization energies for $S_0S_1 \rightarrow T_1T_1$; [d] barrier for $S_0S_1 \rightarrow T_1T_1$.

It is well known that the HOMO-to-LUMO one-electron singlet transition results in a charge resonance state with one of the localized orbitals in Figure 12 being doubly occupied while the other being empty.[114] The charge resonance structures shown in Figure 11(i) correspond to that an electron is depleted from the CAAC on the left side, which contributes the most to the left localized orbital in Figure 12, and the electron is deposited in the C sites on the spacer and the other CAAC that contribute to the right localized orbital in the figure. The charge-resonance structures with the backward electron transfers and symmetry images of all these structures also contribute to the S_1 state, but are not shown in Figure 11(i).

The T_2 state of $(CAAC(F))_2$-Ph corresponds to the HOMO-to-LUMO+1 excitation (see Figure 11(f) for LUMO+1). The ZPE-corrected adiabatic $E(T_2)$ is calculated to be 3.07 eV, giving $\Delta E_{SF}^{(2)} = E(T_2) - 2E(T_1) = 1.09$ eV, satisfying Eq. 2. With $E(T_1)$ @S_1g = 1.20 eV, the reorganization energy for the $S_0S_1 \rightarrow T_1T_1$ fission is estimated to be 0.75 eV, and the barrier is estimated to be 0.02 eV. The less substantial structural reorganizations of the S_1 and T_1 states lead to the half smaller compared to $(CAAC(F))_2$-C_4.

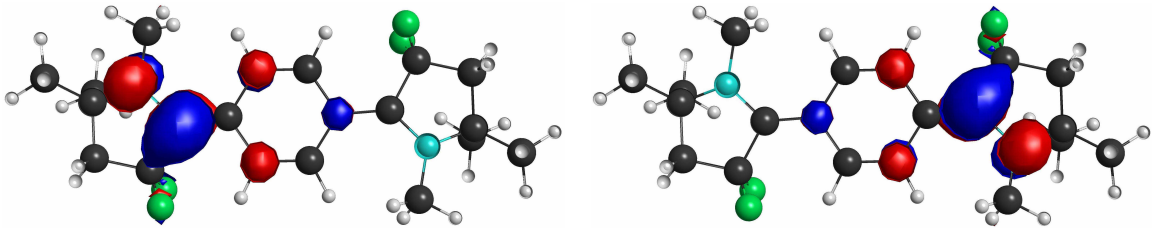

Figure 12. Localized orbitals $(CAAC(F))_2$-Ph obtained from $1/\sqrt{2}$(HOMO ± LUMO)

The smaller λ together with the large positive $\Delta E_{SF}^{(1)}$ result in the essentially barrier-less SF kinetics. The vertical $E(S_1)$ is 2.70 eV with f = 0.85. It corresponds to an intense absorption at the visible region at the solar spectrum that has fairly high photon flux density. Another advantage of $(CAAC(F))_2$-Ph is its 0.99 eV adiabatic $E(T_1)$, which is close to the ~1 eV optimal band gap that maximizes efficiency of a SF-based photovoltaics device.[1,10] With all these advantages, $(CAAC(F))_2$-Ph is a good candidate for SF chromophore.

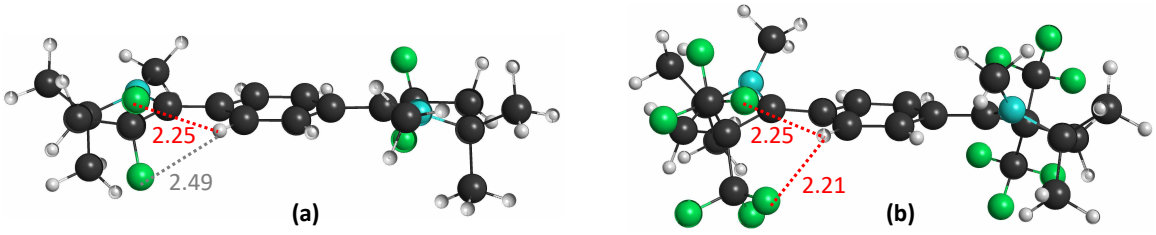

Figure 13. Hydrogen bonds of F atoms in (a) $(CAAC(F))_2$-Ph and (b) $(CAAC(TFM))_2$-Ph. The highlighted internuclear distances are given in Å. The red dashed lines indicate F···H hydrogen bonds.

All those advantages are shared by the (TFM) dimer, which is thus another good candidate. It is interesting that the (TFM) dimer appears to have a higher diradical character than the (F) dimer, indicated by its higher n_{LUNO} = 0.20 and lower vertical $E(T_1)$ = 1.41 eV. This is inconsistent with the expectation based on the electronegativities of TFM and F. We attribute this anomaly to the F···H hydrogen bonds between the F atoms on the CAAC units and the H atoms on the spacer. One of the two highlighted F-H distances shown in Figure 13(a) for the (F) dimer is shorter than the 2.26 Å typical F···H bond distance between a C(sp^3)-F and and a C(sp^2)-H.[115] There is certainly F···H bonding interaction between the CAAC units and the spacer. As shown in Figure 13(b), there are two F-H distances between one CAAC unit and the spacer that are shorter than 2.26 Å. There are thus twice more F···H hydrogen bonds in the (TFM) dimer. This is reasonable as some F atoms of the TFM groups are more oriented towards the spacer. The stronger F···H interaction in the (TFM) dimer requires the CAAC unit to adopt a more preferable configuration for the hydrogen bonds. This results in the larger dihedral angle, d_{NCCC} = 20°, in (CAAC(TFM))$_2$-Ph. The weaker F···H interaction allows a smaller d_{NCCC} = 7° in the (F) dimer, which favors π bonding interaction between the CAAC units and the spacer. The larger dihedral angle in (CAAC(TFM))$_2$-Ph results in less overlap between the carbene π orbitals and the LUMO and HOMO of the spacer, and thus the higher diradical character of (CAAC(TFM))$_2$-Ph.

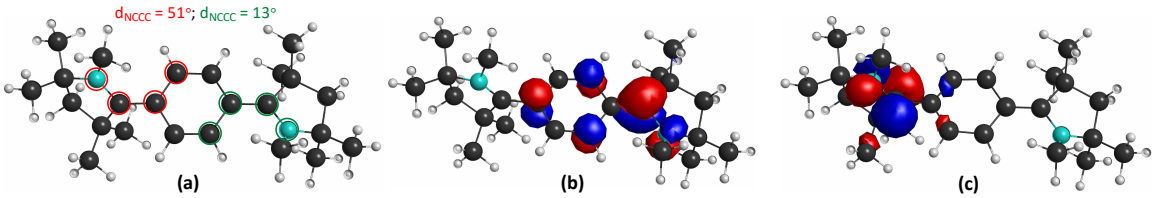

Figure 14. A representative structure (a) obtained during the optimization of the S_1 structure of $(CAAC)_2$-Ph and its (b) HOMO and (c) LUMO.

The 0.43 and 0.62 eV $\Delta E_{SF}^{(1)}$s of $(CAAC(TFM))_2$-Ph and $(CAAC(F))_2$-Ph seem large and imply energy waste and slow SF. However, they are not large when compared with the 0.58 eV $\Delta E_{SF}^{(1)}$ of molecular pentacene. The $\Delta E_{SF}^{(1)}$ of this most intensely studied SF chromophore decreases to 0.11 eV in solid state, due to the significant reduction of its adiabatic $E(S_1)$ from 2.31 to 1.86 eV. This red-shift of $E(S_1)$ in changing from molecules to their crystals is common for organic molecules and is attributed to the Coulomb interaction between neighboring molecules and Davydov splitting.[116] The seemingly large $\Delta E_{SF}^{(1)}$s of the two dimeric molecules have reserved some room for the red-shifts, so that the dimers in solids can still satisfy Eq. 1. Without running solid state calculations, we cannot predict the red-shifts. However, we note that $E(S_1) \approx 2E(T_1)$ may not be an essential requirement for isolated molecules in designing SF chromophores. The approximate isoergicity relation is more relevant for SF in solution or intramolecular SF.

The unsubstituted dimer $(CAAC)_2$-Ph, if all its structures of the four relevant states maintained C_2 symmetry, would also be a possible candidate for SF chromophore. The energies in Table 4 of this dimer are obtained using the C_2 structures. These energies give $\Delta E_{SF}^{(1)}$= -0.03 eV, $\Delta E_{SF}^{(2)}$= 0.20 eV, and a 0.14 eV SF barrier. The non-ZPE-corrected

vertical E*(S1)* and vertical E*(T1)* are calculated to be 2.76 and 1.72 eV, which are in good agreement with the 2.74 and 1.70 eV calculated values reported in Ref. 83. The small negative $\Delta E_{SF}^{(1)}$ can be overcome by thermal activation and the barrier is surmountable. However, the S_1 structure optimized with C_2 symmetry features an imaginary frequency with a symmetry-breaking mode. The optimization following this mode leads to structure with one CAAC unit being significantly non-coplanar with the spacer. One such representative structure is shown in Figure 14(a), with the increased d_{NCCC} angle marked in red color and the other in green color. The HOMO and LUMO of this structure are shown in Figure 14(b) and (c).

At this structure, the S_1 state corresponds to an open-shell singlet with one electron in each of the HOMO and LUMO, while the S_0 state corresponds to double occupation of the HOMO. The S_0-S_1 gap is only 0.24 eV. The two states are about to exchange their characters, and they do a few optimization steps later. The S_1 structural optimization thus failed. Taking $E(S_0)@S_0g$ as the reference, the non-ZPE-corrected E*(S1)* at this structure is calculated to be 2.18 eV, which is substantially less than $2E(T_1) = 2 \times 1.35 = 2.70$ eV. Please note that this $E(T_1)$ does not contain ZPE correction. It is comparable with the non-ZPE-corrected $E(S_1)$. Therefore, even if we can locate the minimum on the S_1 potential energy surface, $(CAAC)_2$-Ph would not satisfy Eq. 1. The S_0-S_1 root flipping in the structural optimization implies that the S_1 would rapidly decay to the S_0 state radiationlessly. The short-lived S_1 also disfavors SF.

The reorganization of the S_1 structure into this asymmetric configuration can be rationalized as follows. As mentioned above, the singlet open-shell with one electron in each of the delocalized HOMO and LUMO in Figure 11(d) and (e) correspond to a

charge resonance closed-shell state, with two electrons in one of the localized orbitals in Figure 12 and none in the other. Such a state features long distance charge transfer between the two CAAA π orbitals (e.g., the first resonance structure in figure 11(i)), which is energy costly. By rotating one CAAC unit out of the plane of the phenylene spacer, the overlap is lost and the delocalized HOMO and LUMO have evolved to the less delocalized HOMO and the localized LUMO in Figure 14s(b) and (c). The singlet open-shell with one electron in each of these resultant orbitals does not involve the long distance charge transfer between the CAAC units. The energy of the S_1 state is hence lower. This tendency to lower the S_1 energy by rotating one CAAC unit out of the plane of the spacer must also be applicable in $(CAAC(TFM)_2$-Ph and $(CAAC(F))_2$-Ph. However, the F···H bonds shown in Figure 13 prevent this distortion from happening.

CHAPTER 4 CONCLUSION

With the objective to design new singlet fission chromophores, we employ MRSF-TDDFT and NEVPT2 methods to investigate a series of cyclic (alkyl)(amino)carbenes (CAAC) dimers. In the dimers, the CAAC units are connected by C_2, C_4, and *p*-phenylene spacers, and they are substituted by trifluoromethyls and fluorine atoms at their α C position. The trifluoromethylation and fluorination are found to stabilize the π LUMO of CAAC, consequently enhance the diradical character for the CAAC dimers, and make them closer to satisfy or satisfy the $E(S_1) \geq 2E(T_1)$ primary energy condition for singlet fission. Meanwhile, the α C remains being a quaternary C. The two substitution schemes will find more use beyond the context of singlet fission, as they can functionalize CAAC in other fields of optoelectronics. The spacers mainly have two effects: (1) the frontier orbitals of a longer spacer (C_4 vs. C_2) are more attenuated and have smaller π overlaps with the orbital of the CAAC units, leading to higher diradical characters of the dimers; (2) cylindrically symmetric spacers C_2 and C_4 allow significant structural reorganizations in the excited states, which potentially lead to endoergicity and high barrier for singlet fission. With both the attenuated frontier orbitals and non-cylindrical symmetry of the spacer, *p*-phenylene-connected dimers with CF_3 and F at the α C position are found to be promising candidates for both thermodynamically and kinetically favorable singlet fission. The presence of the F atoms results in hydrogen bonds between the CAAC units and the spacer. The hydrogen bonds prevent a SF-unfavorable structural distortion in the S_1 state, which occurs in the $(CAAC)_2$-Ph dimer.

Other than proposing the two chromophore candidates, this study demonstrates the importance of considering structural reorganizations in designing singlet fission

chromophores. Considering vertical $E(S_1)$s and adiabatic $E(T_1)$s, all three C_2-connected dimers satisfy $E(S_1) \geq 2E(T_1)$. The significant S_1 structural reorganizations reverse the signs of $E(S_1) - 2E(T_1)$. The structural reorganizations of the S_1 and T_1 states also lead to high barriers for the singlet fission of the C_4-connected trifluoromethylated and the fluorinated dimers. The two dimers, although they satisfy (or close to satisfy) $E(S_1) \geq 2E(T_1)$, are hence not good candidates for singlet fission chromophores. It is a common practice to only consider vertical excitation energies in a quick survey of a large amount of structures in designing singlet fission chromophores. However, it is necessary to consider structural reorganizations of the excited states in order to more conclusively judge whether a molecule is a good candidate.

Reference

1. Smith, M. B. & Michl, J. Singlet Fission. *Chem. Rev.* **110**, 6891–6936 (2010).
2. Smith, M. B. & Michl, J. Recent Advances in Singlet Fission. *Annu. Rev. Phys. Chem.* **64**, 361–386 (2013).
3. Thorsmølle, V. K. *et al.* Morphology Effectively Controls Singlet-Triplet Exciton Relaxation and Charge Transport in Organic Semiconductors. *Phys. Rev. Lett.* **102**, 17401 (2009).
4. Wilson, M. W. B. *et al.* Ultrafast Dynamics of Exciton Fission in Polycrystalline Pentacene. *J. Am. Chem. Soc.* **133**, 11830–11833 (2011).
5. Marciniak, H. *et al.* Ultrafast Exciton Relaxation in Microcrystalline Pentacene Films. *Phys. Rev. Lett.* **99**, 176402 (2007).
6. Chan, W.-L. *et al.* Observing the Multiexciton State in Singlet Fission and Ensuing Ultrafast Multielectron Transfer. *Science (80-.).* **334**, 1541 LP – 1545 (2011).
7. Chan, W.-L., Ligges, M. & Zhu, X.-Y. The energy barrier in singlet fission can be overcome through coherent coupling and entropic gain. *Nat. Chem.* **4**, 840 (2012).
8. Bearpark, M. J. *et al.* The Azulene S1 State Decays via a Conical Intersection: A CASSCF Study with MMVB Dynamics. *J. Am. Chem. Soc.* **118**, 169–175 (1996).
9. Shockley, W. & Queisser, H. J. Detailed balance limit of efficiency of p-n junction solar cells. *J. Appl. Phys.* **32**, 510–519 (1961).
10. Hanna, M. C. & Nozik, A. J. Solar conversion efficiency of photovoltaic and photoelectrolysis cells with carrier multiplication absorbers. *J. Appl. Phys.* **100**, 74510 (2006).
11. Lee, J., Jadhav, P. & Baldo, M. A. High efficiency organic multilayer photodetectors based on singlet exciton fission. *Appl. Phys. Lett.* **95**, 33301 (2009).
12. Congreve, D. N. *et al.* External Quantum Efficiency Above 100% in a Singlet-Exciton-Fission–Based Organic Photovoltaic Cell. *Science (80-.).* **340**, 334 LP – 337 (2013).
13. Thompson, N. J., Congreve, D. N., Goldberg, D., Menon, V. M. & Baldo, M. A. Slow light enhanced singlet exciton fission solar cells with a 126% yield of electrons per photon. *Appl. Phys. Lett.* **103**, 263302 (2013).
14. Pazos-Outón, L. M. *et al.* A Silicon–Singlet Fission Tandem Solar Cell Exceeding 100% External Quantum Efficiency with High Spectral Stability. *ACS Energy Lett.* **2**, 476–480 (2017).
15. Sanders, S. N. *et al.* Intramolecular Singlet Fission in Oligoacene Heterodimers. *Angew. Chemie Int. Ed.* **55**, 3373–3377 (2016).
16. Xia, J. *et al.* Singlet Fission: Progress and Prospects in Solar Cells. *Adv. Mater.* **29**, 1601652 (2017).
17. Piland, G. B., Burdett, J. J., Dillon, R. J. & Bardeen, C. J. Singlet Fission: From Coherences to Kinetics. *J. Phys. Chem. Lett.* **5**, 2312–2319 (2014).
18. Scholes, G. D. Correlated Pair States Formed by Singlet Fission and Exciton–Exciton Annihilation. *J. Phys. Chem. A* **119**, 12699–12705 (2015).
19. Tayebjee, M. J. Y. *et al.* Quintet multiexciton dynamics in singlet fission. *Nat. Phys.* **13**, 182 (2016).
20. Basel, B. S. *et al.* Unified model for singlet fission within a non-conjugated covalent pentacene dimer. *Nat. Commun.* **8**, 15171 (2017).

21. Tempelaar, R. & Reichman, D. R. Vibronic exciton theory of singlet fission. I. Linear absorption and the anatomy of the correlated triplet pair state. *J. Chem. Phys.* **146**, 174703 (2017).
22. Kolomeisky, A. B., Feng, X. & Krylov, A. I. A Simple Kinetic Model for Singlet Fission: A Role of Electronic and Entropic Contributions to Macroscopic Rates. *J. Phys. Chem. C* **118**, 5188–5195 (2014).
23. Peierls, R. E. *Quantum Theory of Solids*. (Clarendon Press, 1996).
24. Tamura, H., Huix-Rotllant, M., Burghardt, I., Olivier, Y. & Beljonne, D. First-Principles Quantum Dynamics of Singlet Fission: Coherent versus Thermally Activated Mechanisms Governed by Molecular $\ensuremath{\pi}$ Stacking. *Phys. Rev. Lett.* **115**, 107401 (2015).
25. Singh, S., Jones, W. J., Siebrand, W., Stoicheff, B. P. & Schneider, W. G. Laser Generation of Excitons and Fluorescence in Anthracene Crystals. *J. Chem. Phys.* **42**, 330–342 (1965).
26. Swenberg, C. E. & Stacy, W. T. Bimolecular radiationless transitions in crystalline tetracene. *Chem. Phys. Lett.* **2**, 327–328 (1968).
27. Geacintov, N., Pope, M. & Vogel, F. Effect of Magnetic Field on the Fluorescence of Tetracene Crystals: Exciton Fission. *Phys. Rev. Lett.* **22**, 593–596 (1969).
28. Groff, R. P., Avakian, P. & Merrifield, R. E. Coexistence of Exciton Fission and Fusion in Tetracene Crystals. *Phys. Rev. B* **1**, 815–817 (1970).
29. Swenberg, C. E., van Metter, R. & Ratner, M. Comments on exciton fission and electron spin resonance in tetracene single crystals. *Chem. Phys. Lett.* **16**, 482–485 (1972).
30. Burgos, J., Pope, M., Swenberg, C. E. & Alfano, R. R. Heterofission in pentacene-doped tetracene single crystals. *Phys. status solidi* **83**, 249–256 (1977).
31. Tomkiewicz, Y., Groff, R. P. & Avakian, P. Spectroscopic Approach to Energetics of Exciton Fission and Fusion in Tetracene Crystals. *J. Chem. Phys.* **54**, 4504–4507 (1971).
32. Burdett, J. J., Müller, A. M., Gosztola, D. & Bardeen, C. J. Excited state dynamics in solid and monomeric tetracene: The roles of superradiance and exciton fission. *J. Chem. Phys.* **133**, 144506 (2010).
33. Burdett, J. J., Gosztola, D. & Bardeen, C. J. The dependence of singlet exciton relaxation on excitation density and temperature in polycrystalline tetracene thin films: Kinetic evidence for a dark intermediate state and implications for singlet fission. *J. Chem. Phys.* **135**, 214508 (2011).
34. Burdett, J. J. & Bardeen, C. J. Quantum Beats in Crystalline Tetracene Delayed Fluorescence Due to Triplet Pair Coherences Produced by Direct Singlet Fission. *J. Am. Chem. Soc.* **134**, 8597–8607 (2012).
35. Roberts, S. T. *et al.* Efficient Singlet Fission Discovered in a Disordered Acene Film. *J. Am. Chem. Soc.* **134**, 6388–6400 (2012).
36. Mastron, J. N., Roberts, S. T., McAnally, R. E., Thompson, M. E. & Bradforth, S. E. Aqueous Colloidal Acene Nanoparticles: A New Platform for Studying Singlet Fission. *J. Phys. Chem. B* **117**, 15519–15526 (2013).
37. Najafov, H., Lee, B., Zhou, Q., Feldman, L. C. & Podzorov, V. Observation of long-range exciton diffusion in highly ordered organic semiconductors. *Nat. Mater.* **9**, 938 (2010).

38. Ryasnyanskiy, A. & Biaggio, I. Triplet exciton dynamics in rubrene single crystals. *Phys. Rev. B* **84**, 193203 (2011).
39. Jankus, V. *et al.* Competition between polaron pair formation and singlet fission observed in amorphous rubrene films. *Phys. Rev. B* **87**, 224202 (2013).
40. Rao, A. *et al.* Exciton Fission and Charge Generation via Triplet Excitons in Pentacene/C60 Bilayers. *J. Am. Chem. Soc.* **132**, 12698–12703 (2010).
41. Rao, A., Wilson, M. W. B., Albert-Seifried, S., Di Pietro, R. & Friend, R. H. Photophysics of pentacene thin films: The role of exciton fission and heating effects. *Phys. Rev. B* **84**, 195411 (2011).
42. Ramanan, C., Smeigh, A. L., Anthony, J. E., Marks, T. J. & Wasielewski, M. R. Competition between Singlet Fission and Charge Separation in Solution-Processed Blend Films of 6,13-Bis(triisopropylsilylethynyl)pentacene with Sterically-Encumbered Perylene-3,4:9,10-bis(dicarboximide)s. *J. Am. Chem. Soc.* **134**, 386–397 (2012).
43. Walker, B. J., Musser, A. J., Beljonne, D. & Friend, R. H. Singlet exciton fission in solution. *Nat. Chem.* **5**, 1019 (2013).
44. Eaton, S. W. *et al.* Singlet Exciton Fission in Polycrystalline Thin Films of a Slip-Stacked Perylenediimide. *J. Am. Chem. Soc.* **135**, 14701–14712 (2013).
45. Busby, E. *et al.* A design strategy for intramolecular singlet fission mediated by charge-transfer states in donor–acceptor organic materials. *Nat. Mater.* **14**, 426 (2015).
46. Kraabel, B., Hulin, D., Aslangul, C., Lapersonne-Meyer, C. & Schott, M. Triplet exciton generation, transport and relaxation in isolated polydiacetylene chains: Subpicosecond pump-probe experiments. *Chem. Phys.* **227**, 83–98 (1998).
47. Gradinaru, C. C. *et al.* An unusual pathway of excitation energy deactivation in carotenoids: Singlet-to-triplet conversion on an ultrafast timescale in a photosynthetic antenna. *Proc. Natl. Acad. Sci.* **98**, 2364 LP – 2369 (2001).
48. Wang, C., Schlamadinger, D. E., Desai, V. & Tauber, M. J. Triplet Excitons of Carotenoids Formed by Singlet Fission in a Membrane. *ChemPhysChem* **12**, 2891–2894 (2011).
49. Wang, C. & Tauber, M. J. High-Yield Singlet Fission in a Zeaxanthin Aggregate Observed by Picosecond Resonance Raman Spectroscopy. *J. Am. Chem. Soc.* **132**, 13988–13991 (2010).
50. Musser, A. J. *et al.* Activated Singlet Exciton Fission in a Semiconducting Polymer. *J. Am. Chem. Soc.* **135**, 12747–12754 (2013).
51. Kawata, S. *et al.* Singlet Fission of Non-polycyclic Aromatic Molecules in Organic Photovoltaics. *Adv. Mater.* **28**, 1585–1590 (2016).
52. Kasha, M. Characterization of electronic transitions in complex molecules. *Discuss. Faraday Soc.* **9**, 14–19 (1950).
53. Lower, S. K. & El-Sayed, M. A. The triplet state and molecular electronic processes in organic molecules. *Chem. Rev.* **66**, 199–241 (1966).
54. El-Sayed, M. A. Triplet state. Its radiative and nonradiative properties. *Acc. Chem. Res.* **1**, 8–16 (1968).
55. Paci, I. *et al.* Singlet Fission for Dye-Sensitized Solar Cells: Can a Suitable Sensitizer Be Found? *J. Am. Chem. Soc.* **128**, 16546–16553 (2006).
56. Bendikov, M. *et al.* Oligoacenes: theoretical prediction of open-shell singlet

diradical ground states. *J. Am. Chem. Soc.* **126**, 7416–7417 (2004).
57. Hachmann, J., Dorando, J. J., Avilés, M. & Chan, G. K.-L. The radical character of the acenes: A density matrix renormalization group study. *J. Chem. Phys.* **127**, 134309 (2007).
58. Yang, Y., Davidson, E. R. & Yang, W. Nature of ground and electronic excited states of higher acenes. *Proc. Natl. Acad. Sci.* **113**, E5098–E5107 (2016).
59. Pariser, R. & Parr, R. G. A Semi-Empirical Theory of the Electronic Spectra and Electronic Structure of Complex Unsaturated Molecules. I. *J. Chem. Phys.* **21**, 466–471 (1953).
60. Pople, J. A. Electron interaction in unsaturated hydrocarbons. *Trans. Faraday Soc.* **49**, 1375–1385 (1953).
61. Johnson, J. C., Nozik, A. J. & Michl, J. High triplet yield from singlet fission in a thin film of 1, 3-diphenylisobenzofuran. *J. Am. Chem. Soc.* **132**, 16302–16303 (2010).
62. Ryerson, J. L. *et al.* Two thin film polymorphs of the singlet fission compound 1, 3-diphenylisobenzofuran. *J. Phys. Chem. C* **118**, 12121–12132 (2014).
63. Schrauben, J. N., Ryerson, J. L., Michl, J. & Johnson, J. C. Mechanism of singlet fission in thin films of 1, 3-diphenylisobenzofuran. *J. Am. Chem. Soc.* **136**, 7363–7373 (2014).
64. Schwerin, A. F. *et al.* Toward designed singlet fission: electronic states and photophysics of 1, 3-diphenylisobenzofuran. *J. Phys. Chem. A* **114**, 1457–1473 (2009).
65. Johnson, J. C. & Michl, J. 1, 3-Diphenylisobenzofuran: a Model Chromophore for Singlet Fission. in *Physical Organic Chemistry of Quinodimethanes* 249–277 (Springer, 2017).
66. Minami, T. & Nakano, M. Diradical character view of singlet fission. *J. Phys. Chem. Lett.* **3**, 145–150 (2011).
67. Ito, S. & Nakano, M. Theoretical Molecular Design of Heteroacenes for Singlet Fission: Tuning the Diradical Character by Modifying π-Conjugation Length and Aromaticity. *J. Phys. Chem. C* **119**, 148–157 (2015).
68. Ito, S., Nagami, T. & Nakano, M. Diradical Character-Based Design for Singlet Fission of Bisanthene Derivatives: Aromatic-Ring Attachment and π-Plane Twisting. *J. Phys. Chem. Lett.* **7**, 3925–3930 (2016).
69. Akdag, A., Havlas, Z. & Michl, J. Search for a small chromophore with efficient singlet fission: biradicaloid heterocycles. *J. Am. Chem. Soc.* **134**, 14624–14631 (2012).
70. Viehe, H. G., Janousek, Z., Merenyi, R. & Stella, L. The captodative effect. *Acc. Chem. Res.* **18**, 148–154 (1985).
71. Zeng, T., Ananth, N. & Hoffmann, R. Seeking small molecules for singlet fission: a heteroatom substitution strategy. *J. Am. Chem. Soc.* **136**, 12638–12647 (2014).
72. Campbell, P. G., Marwitz, A. J. V & Liu, S. Recent advances in azaborine chemistry. *Angew. Chemie Int. Ed.* **51**, 6074–6092 (2012).
73. Wen, J., Havlas, Z. Z. & Michl, J. Captodatively stabilized biradicaloids as chromophores for singlet fission. *J. Am. Chem. Soc.* **137**, 165–172 (2014).
74. Bhattacharyya, K., Pratik, S. M. & Datta, A. Small organic molecules for efficient singlet fission: role of silicon substitution. *J. Phys. Chem. C* **119**, 25696–25702

(2015).
75. Würfel, P. & Würfel, U. *Physics of solar cells: from basic principles to advanced concepts*. (John Wiley & Sons, 2016).
76. Zeng, T., Hoffmann, R. & Ananth, N. The low-lying electronic states of pentacene and their roles in singlet fission. *J. Am. Chem. Soc.* **136**, 5755–5764 (2014).
77. Minami, T., Ito, S. & Nakano, M. Fundamental of Diradical-Character-Based Molecular Design for Singlet Fission. *J. Phys. Chem. Lett.* **4**, 2133–2137 (2013).
78. Ito, S., Nagami, T. & Nakano, M. Molecular design for efficient singlet fission. *J. Photochem. Photobiol. C Photochem. Rev.* **34**, 85–120 (2018).
79. Japahuge, A. & Zeng, T. Theoretical Studies of Singlet Fission: Searching for Materials and Exploring Mechanisms. *Chempluschem* **83**, 146–182 (2018).
80. Zeng, T. & Goel, P. Design of Small Intramolecular Singlet Fission Chromophores: An Azaborine Candidate and General Small Size Effects. *J. Phys. Chem. Lett.* **7**, 1351–1358 (2016).
81. Zeng, T. Through-Linker Intramolecular Singlet Fission: General Mechanism and Designing Small Chromophores. *J. Phys. Chem. Lett.* **7**, 4405–4412 (2016).
82. Zeng, T. *et al.* Identifying (BN)2-pyrenes as a New Class of Singlet Fission Chromophores: Significance of Azaborine Substitution. *J. Phys. Chem. Lett.* **9**, 2919–2927 (2018).
83. Messelberger, J., Grünwald, A., Pinter, P., Hansmann, M. M. & Munz, D. Carbene derived diradicaloids - building blocks for singlet fission? *Chem. Sci.* **9**, 6107–6117 (2018).
84. Soleilhavoup, M. & Bertrand, G. Cyclic (Alkyl)(Amino)Carbenes (CAACs): Stable Carbenes on the Rise. *Acc. Chem. Res.* **48**, 256–266 (2015).
85. Hansmann, M. M., Melaimi, M., Munz, D. & Bertrand, G. Modular Approach to Kekulé Diradicaloids Derived from Cyclic (Alkyl)(amino)carbenes. *J. Am. Chem. Soc.* **140**, 2546–2554 (2018).
86. Kinjo, R., Donnadieu, B. & Bertrand, G. Isolation of a Carbene-Stabilized Phosphorus Mononitride and Its Radical Cation (PN+.). *Angew. Chemie Int. Ed.* **49**, 5930–5933 (2010).
87. Back, O., Donnadieu, B., Parameswaran, P., Frenking, G. & Bertrand, G. Isolation of crystalline carbene-stabilized P2-radical cations and P2-dications. *Nat. Chem.* **2**, 369 (2010).
88. Back, O. *et al.* A Crystalline Phosphinyl Radical Cation. *J. Am. Chem. Soc.* **132**, 10262–10263 (2010).
89. Kinjo, R., Donnadieu, B., Celik, M. A., Frenking, G. & Bertrand, G. Synthesis and Characterization of a Neutral Tricoordinate Organoboron Isoelectronic with Amines. *Science (80-.).* **333**, 610 LP – 613 (2011).
90. Lavallo, V., Canac, Y., Präsang, C., Donnadieu, B. & Bertrand, G. Stable cyclic (alkyl)(amino)carbenes as rigid or flexible, bulky, electron-rich ligands for transition-metal catalysts: a quaternary carbon atom makes the difference. *Angew. Chem. Int. Ed. Engl.* **44**, 5705–5709 (2005).
91. Pasto, D. J. Radical stabilization energies of disubstituted methyl radicals. A detailed theoretical analysis of the captodative effect. *J. Am. Chem. Soc.* **110**, 8164–8175 (1988).
92. Lee, S. S., Filatov, M., Lee, S. S. & Choi, C. H. Eliminating spin-contamination of

spin-flip time dependent density functional theory within linear response formalism by the use of zeroth-order mixed-reference (MR) reduced density matrix. *J. Chem. Phys.* **149**, 104101 (2018).
93. Lee, S. S. *et al.* Efficient implementations of analytic energy gradient for mixed-reference spin-flip time-dependent density functional theory (MRSF-TDDFT). *J. Chem. Phys.* **150**, 184111 (2019).
94. Lee, C., Yang, W. & Parr, R. G. Development of the Colle-Salvetti correlation-energy formula into a functional of the electron density. *Phys. Rev. B* **37**, 785–789 (1988).
95. Becke, A. D. Density-functional thermochemistry. III. The role of exact exchange. *J. Chem. Phys.* **98**, 5648–5652 (1993).
96. Weigend, F. & Ahlrichs, R. Balanced basis sets of split valence, triple zeta valence and quadruple zeta valence quality for H to Rn: Design and assessment of accuracy. *Phys. Chem. Chem. Phys.* **7**, 3297–3305 (2005).
97. Schmidt, M. W. *et al.* General atomic and molecular electronic structure system. *J. Comput. Chem.* **14**, 1347–1363 (1993).
98. Gordon, M. S. & Schmidt, M. W. Chapter 41 - Advances in electronic structure theory: GAMESS a decade later. in (eds. Dykstra, C. E., Frenking, G., Kim, K. S. & Scuseria, G. E. B. T.-T. and A. of C. C.) 1167–1189 (Elsevier, 2005). doi:https://doi.org/10.1016/B978-044451719-7/50084-6
99. Brédas, J.-L., Beljonne, D., Coropceanu, V. & Cornil, J. Charge-Transfer and Energy-Transfer Processes in π-Conjugated Oligomers and Polymers: A Molecular Picture. *Chem. Rev.* **104**, 4971–5004 (2004).
100. Volkhard, M. & Oliver, K. *No Title*. (2003). doi:doi:10.1002/9783527602575
101. Navarro, A. *et al.* Effect of five-membered ring and heteroatom substitution on charge transport properties of perylene discotic derivatives: A theoretical approach. *J. Chem. Phys.* **145**, 54903 (2016).
102. Angeli, C., Cimiraglia, R., Evangelisti, S., Leininger, T. & Malrieu, J.-P. Introduction of n-electron valence states for multireference perturbation theory. *J. Chem. Phys.* **114**, 10252–10264 (2001).
103. Angeli, C., Cimiraglia, R. & Malrieu, J.-P. n-electron valence state perturbation theory: A spinless formulation and an efficient implementation of the strongly contracted and of the partially contracted variants. *J. Chem. Phys.* **117**, 9138–9153 (2002).
104. Neese, F. The ORCA program system. *Wiley Interdiscip. Rev. Comput. Mol. Sci.* **2**, 73–78 (2012).
105. Mayer, I. Bond order and valence: Relations to Mulliken's population analysis. *Int. J. Quantum Chem.* **26**, 151–154 (1984).
106. Hoffmann, R. Interaction of orbitals through space and through bonds. *Acc. Chem. Res.* **4**, 1–9 (1971).
107. Ozimiński, W. P. & Dobrowolski, J. C. σ- and π-electron contributions to the substituent effect: natural population analysis. *J. Phys. Org. Chem.* **22**, 769–778 (2009).
108. Rahm, M., Zeng, T. & Hoffmann, R. Electronegativity Seen as the Ground-State Average Valence Electron Binding Energy. *J. Am. Chem. Soc.* **141**, 342–351 (2018).

109. True, J. E., Thomas, T. D., Winter, R. W. & Gard, G. L. Electronegativities from core-ionization energies: electronegativities of SF5 and CF3. *Inorg. Chem.* **42**, 4437–4441 (2003).
110. Jin, L., Melaimi, M., Liu, L. & Bertrand, G. Singlet carbenes as mimics for transition metals: synthesis of an air stable organic mixed valence compound [M 2 (C 2)+˙; M= cyclic (alkyl)(amino) carbene]. *Org. Chem. Front.* **1**, 351–354 (2014).
111. Li, Y. *et al.* C4 Cumulene and the Corresponding Air-Stable Radical Cation and Dication. *Angew. Chemie Int. Ed.* **53**, 4168–4172 (2014).
112. Flynn, C. R. & Michl, J. . pi.,. pi.-Biradicaloid hydrocarbons. o-Xylylene. Photochemical preparation from 1, 4-dihydrophthalazine in rigid glass, electric spectroscopy, and calculations. *J. Am. Chem. Soc.* **96**, 3280–3288 (1974).
113. Marcus, R. A. Electron transfer reactions in chemistry. Theory and experiment. *Rev. Mod. Phys.* **65**, 599 (1993).
114. Shaik, S. S. & Hiberty, P. C. *A chemist's guide to valence bond theory*. (John Wiley & Sons, 2007).
115. Prakash, G. K. S. *et al.* On the Nature of C□ H··· F□ C Interactions in Hindered CF3□ C (sp3) Bond Rotations. *Angew. Chemie Int. Ed.* **50**, 11761–11764 (2011).
116. Schwoerer, M. & Wolf, H. C. *Organic molecular solids*. (John Wiley & Sons, 2007).